AGU PUBLICATIONS

Paleoceanography

RESEARCH ARTICLE
10.1002/2017PA003197

Key Points:
- Published $^{40}Ar/^{39}Ar$ data from biotite-rich layers from the Umbria-Marche sedimentary succession too old by approximately 0.5 Myr
- U-Pb (zircon) dating of the Umbria-Marche biotite-rich layers in agreement with the astronomically tuned Oligocene time scale
- New U-Pb calibrated age for the Eocene-Oligocene boundary (34.09 ± 0.08 Ma) and the Rupelian-Chattian boundary (28.11 ± 0.17 Ma)

Supporting Information:
- Supporting Information S1
- Table S2
- Table S3
- Table S4
- Table S5

Correspondence to:
D. Sahy,
dihy@bgs.ac.uk

Citation:
Sahy, D., Condon, D. J., Hilgen, F. J., & Kuiper, K. F. (2017). Reducing disparity in radio-isotopic and astrochronology-based time scales of the late Eocene and Oligocene. *Paleoceanography*, *32*, 1018–1035. https://doi.org/10.1002/2017PA003197

Received 26 JUN 2017
Accepted 13 SEP 2017
Accepted article online 24 SEP 2017
Published online 20 OCT 2017

Reducing Disparity in Radio-Isotopic and Astrochronology-Based Time Scales of the Late Eocene and Oligocene

Diana Sahy[1], Daniel J. Condon[1], Frederik J. Hilgen[2], and Klaudia F. Kuiper[2,3]

[1]NERC Isotope Geosciences Laboratory, British Geological Survey, Keyworth, UK, [2]Department of Earth Science, Utrecht University, Utrecht, Netherlands, [3]Faculty of Earth and Life Sciences, Department of Earth Sciences, Vrije Universiteit Amsterdam, Amsterdam, Netherlands

Abstract A significant discrepancy of up to 0.6 Myr exists between radio-isotopically calibrated and astronomically tuned time scales of the late Eocene-Oligocene. We explore the possible causes of this discrepancy through the acquisition of "high-precision" $^{206}Pb/^{238}U$ dating of zircons from 11 volcanic ash beds from the Umbria-Marche sedimentary succession, which hosts the Global Stratotype Section and Point for the base of the Oligocene. Our results indicate that the four $^{40}Ar/^{39}Ar$ dates from the Umbria-Marche succession, which underpin the late Eocene-Oligocene portion of the Paleogene geomagnetic polarity time scale in the 2012 edition of the Geological Time Scale, are anomalously old by up to 0.5 Myr. Conversely, when integrated with the established magnetic polarity record of the Umbria-Marche succession, $^{206}Pb/^{238}U$ (zircon) data from this study result in Oligocene magnetic reversal ages that are generally equivalent to those obtained through the tuning of Ocean Drilling Program (ODP) Site 1218 (equatorial Pacific). Furthermore, our results indicate that the late Eocene tuning of ODP Site 1218, and International Ocean Discovery Program (IODP) Sites U1333–1334 (equatorial Pacific), to the 405 kyr eccentricity signal is accurate, at least back to 36 Ma. Propagating the full uncertainty of our radio-isotopic data set and, where appropriate, taking into account locally derived astronomical time scales, we arrive at an age of 34.09 ± 0.08 Ma for the Eocene-Oligocene boundary and 28.11 ± 0.17 Ma for the base of the Chattian.

1. Introduction

The Paleogene was a time of significant and often abrupt climate change, punctuated by Paleocene-Eocene hyperthermals (Zachos et al., 2001), the inception of a continent-scale Antarctic ice sheet at the Eocene-Oligocene transition (Shackleton & Kennett, 1975), and astronomically controlled Oligocene climate fluctuations (Liebrand et al., 2016; Pälike et al., 2006). Quantifying the rates and timing of environmental change relative to potential forcing mechanisms such as volcanic eruptions, tectonic changes, or orbital configurations, and the evaluation of leads and lags between different depositional settings, requires age models derived from accurate and precise age constraints. The methods of choice for deriving such absolute age constraints from Paleogene records are $^{40}Ar/^{39}Ar$ dating of sanidine and $^{206}Pb/^{238}U$ dating of zircon from syndepositional volcanic tuffs and astronomical tuning. However, much of the Paleogene sedimentary record is not amenable to direct dating due to the lack of suitable volcanic tuffs and/or difficulties in identifying eccentricity, obliquity, and where applicable, precession cycles in proxy data sets due to the presence of hiatuses or fluctuations in sediment accumulation rates. The geomagnetic polarity time scale (GPTS) provides a means for the relative dating of such records, through the identification of magnetic reversals of known age, or bioevents whose calibration relative to the GPTS is known. In turn, the age calibration of the GPTS itself traditionally relies on interpolation along a synthetic marine magnetic anomaly profile (e.g., South Atlantic; Cande & Kent, 1992) using a selection of published radio-isotopic dates considered to be both analytically robust and magnetostratigraphically well calibrated (radio-isotopically calibrated GPTS, hereafter RI-GPTS; e.g., Cande & Kent, 1992, 1995; Berggren et al., 1985; Ogg & Smith, 2004; Vandenberghe et al., 2012). However, except for the vicinity of the Cretaceous-Paleogene boundary (Kuiper et al., 2008; Renne et al., 2013; Swisher, Dingus, & Butler, 1993), the Paleocene-Eocene thermal maximum (e.g., Charles et al., 2011), and the Eocene-Oligocene boundary (Coccioni et al., 2008; Odin et al., 1991; Odin et al., 1991; Sahy et al., 2015; Swisher & Prothero, 1990), the Paleogene is relatively poorly constrained (Figure 1). Additionally, some published data sets were obtained on biotite, a less than ideal geochronometer for time scale calibration, due to its tendency to include extraneous ^{40}Ar (Hora et al., 2010) and/or on multigrain fractions of the mineral of interest (e.g.,

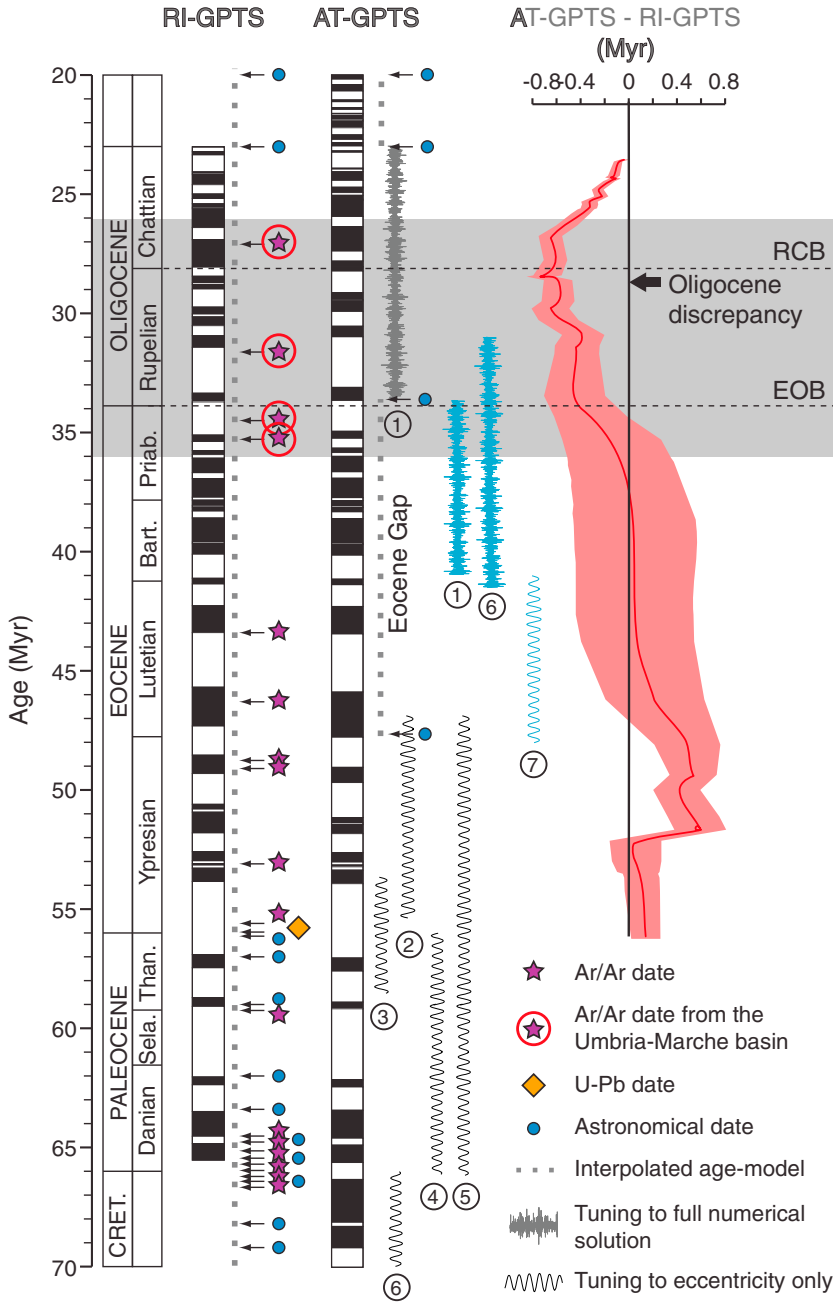

Figure 1. Summary of data used to calibrate the radio-isotopic (RI-GPTS) and astronomically tuned (AT-GPTS) Paleogene time scales in GTS12. Gray rectangle marks the time interval covered in this study, with the Eocene-Oligocene boundary (EOB), Rupelian-Chattian boundary (RCB), and the Oligocene discrepancy, centered on 28 Ma between the RI-GPTS and AT-GPTS highlighted. The records included in the AT-GPTS are 1 = ODP Site 1218 (Pälike et al., 2006); 2 = Demerara Rise (Westerhold & Röhl, 2009); 3 = Walvis Ridge (Westerhold et al., 2007); 4 = Shatsky Rise (Westerhold et al., 2008); 5 = revised tuning of records 2, 3, and 4 by Hilgen et al. (2010). Also shown is the extent of the Eocene gap in the AT-GPTS, and the main tuning options which can be used to narrow the gap: 1 = as above, 6 = Pacific equatorial age transect of Westerhold et al. (2013), 7 = ODP sites 702 and 1263 (Westerhold et al., 2015). Note that the symbols used to represent astronomically tuned records are not to scale.

Odin et al., 1991), which may be masking geological scatter that is resolvable with state-of-the-art methodologies. The wide spacing of the available radio-isotopic dates also implies that the choice of interpolation method may have a resolvable impact on the GPTS and that interpolated age uncertainties are large (i.e., >1%) compared to the precision of the radio-isotopic tie points.

The astronomical tuning of deep marine records spanning several million years has emerged as a viable alternative for the calibration of the Paleogene GPTS (astronomically tuned GPTS, hereafter AT-GPTS). Tuning has the advantage of producing continuous age models, with a theoretical precision on the order of 0.1%, and thus sidesteps both the possible interpolation-related artefacts and large uncertainties typically associated with the RI-GPTS. However, to achieve complete coverage of the Paleogene, the AT-GPTS has to rely on a compilation of multiple individually tuned proxy records and magnetic polarity patterns from different localities (e.g., Vandenberghe et al., 2012) (Figure 1). Consequently, the accuracy of the AT-GPTS is subject to the complete expression and accurate identification of Milankovitch cycles at each locality, the validity of the correlations between different localities, and the validity of correlation of observed cycles to insolation targets. These factors can be evaluated either by comparing multiple tuned records of the same time interval or through comparisons with radio-isotopic dates from volcanic tuffs intercalated in magnetostratigraphically well calibrated sedimentary successions, using concordance between multiple records and/or dating methods as a test of accuracy. In order to facilitate such comparisons, considerable effort has been invested into refining both the numerical solutions that underpin astronomical tuning (Laskar et al., 2004; Laskar et al., 2011) and radio-isotopic dating methods based on the $^{40}Ar/^{39}Ar$ and $^{206}Pb/^{238}U$ systems (Condon et al., 2015; Kuiper et al., 2008; Mattinson, 2005; McLean et al., 2015; Min et al., 2000; Renne et al., 1994, 1998; Renne et al., 2010; Rivera et al., 2011), partly through international, community-driven initiatives (e.g., EARTHTIME and EARTHTIME-EU). In spite of this, the most recent 2012 edition of the Geological Time Scale (GTS12) revealed discrepancies of up to 0.6 Myr between the RI-GPTS and AT-GPTS (Figure 1) in the Oligocene and early Eocene (Vandenberghe et al., 2012).

The Oligocene discrepancy between the RI-GPTS and AT-GPTS of GTS12 extends between 33 and 25 Ma (Figure 1) and arises from a comparison between $^{40}Ar/^{39}Ar$ dates from the Umbria-Marche sedimentary succession in central Italy (Coccioni et al., 2008; Odin et al., 1991) and the tuning of proxy data from Ocean Drilling Program (ODP) Site 1218 in the equatorial Pacific (Pälike et al., 2006; 0–41 Ma, hereafter ATPS06) to the full numerical solution of Laskar et al. (2004) (hereafter La2004).

Rb-Sr, K-Ar, and/or $^{40}Ar/^{39}Ar$ dates sourced from centimeter-thick distal air fall tuffs deposited in a pelagic environment in the Umbria-Marche basin (Montanari et al., 1988, 1985; Odin et al., 1991; Odin et al., 1991), often referred to as biotite-rich layers (BRLs), have been used to constrain the Eocene-Oligocene in most recent RI-GPTS (Cande & Kent, 1992, 1995; Berggren et al., 1985; Ogg & Smith, 2004; Vandenberghe et al., 2012). Four such multigrain biotite $^{40}Ar/^{39}Ar$ dates were included in GTS12, two from BRL intercalated in the Massignano section (Odin et al., 1991) (Figure 2), which hosts the Global Stratotype Section and Point (GSSP) for the base of the Oligocene (Premoli Silva & Jenkins, 1993), and two from the Monte Cagnero section (Coccioni et al., 2008) (Figure 2), a proposed site for the GSSP of the Chattian.

The accuracy of $^{40}Ar/^{39}Ar$ dates depends on the complexity of the analyzed samples, the ^{40}K decay constant, and the assumed age of mineral standards used (commonly Fish Canyon sanidine (FCs)). GTS12 adopted an FCs age of 28.201 ± 0.046 Ma (Kuiper et al., 2008) and a ^{40}K decay constant of $0.5463 \pm 0.0107 \times 10^{-9}$ years (Min et al., 2000), and the same values are used in this study. A FCs age of approximately 28.2 Ma is supported by intercalibration experiments relative to astronomically tuned records (Kuiper et al., 2008; Rivera et al., 2011) and the measurement optimization approach of Renne et al. (2010) as well as independent $^{206}Pb/^{238}U$ dating of zircons from the Fish Canyon tuff itself (Wotzlaw et al., 2013). The implication is that the choice of FCs age in GTS12 is unlikely to result in significant systematic bias in the RI-GPTS and that earlier RI-GPTS (e.g., Cande & Kent, 1995; Ogg & Smith, 2004), which used data reported relative to younger FCs ages of 27.84 Ma (Renne et al., 1994) and 28.02 Ma (Renne et al., 1998), are effectively obsolete.

Part of the ATPS06 underpins the tuning of the Oligocene in GTS12 between 23.0 and 33.7 Ma and is linked to the astronomically tuned Neogene time scale by an Oligocene-Miocene boundary age (23.024 Ma) closely matching that obtained in the Carrosio-Lemme section through magneto-biostratigraphic constraints (23.03 Ma; Shackleton et al., 2000; Lourens et al., 2004). Biotite and anorthoclase $^{40}Ar/^{39}Ar$ dates from volcanic tuffs intercalated in the terrestrial White River Group in North America (Swisher & Prothero, 1990) have previously been cited as potential indicators of a missing 405 kyr cycle in the Oligocene portion of the ATPS06 (Hilgen & Kuiper, 2009). However, more recent $^{206}Pb/^{238}U$ dating of zircons from the same White River tuffs supports the tuning of the ATPS06, at least at the level of the 405 kyr eccentricity cycles, with published anomalously old $^{40}Ar/^{39}Ar$ data attributed to the presence of detrital biotite and anorthoclase grains (Sahy

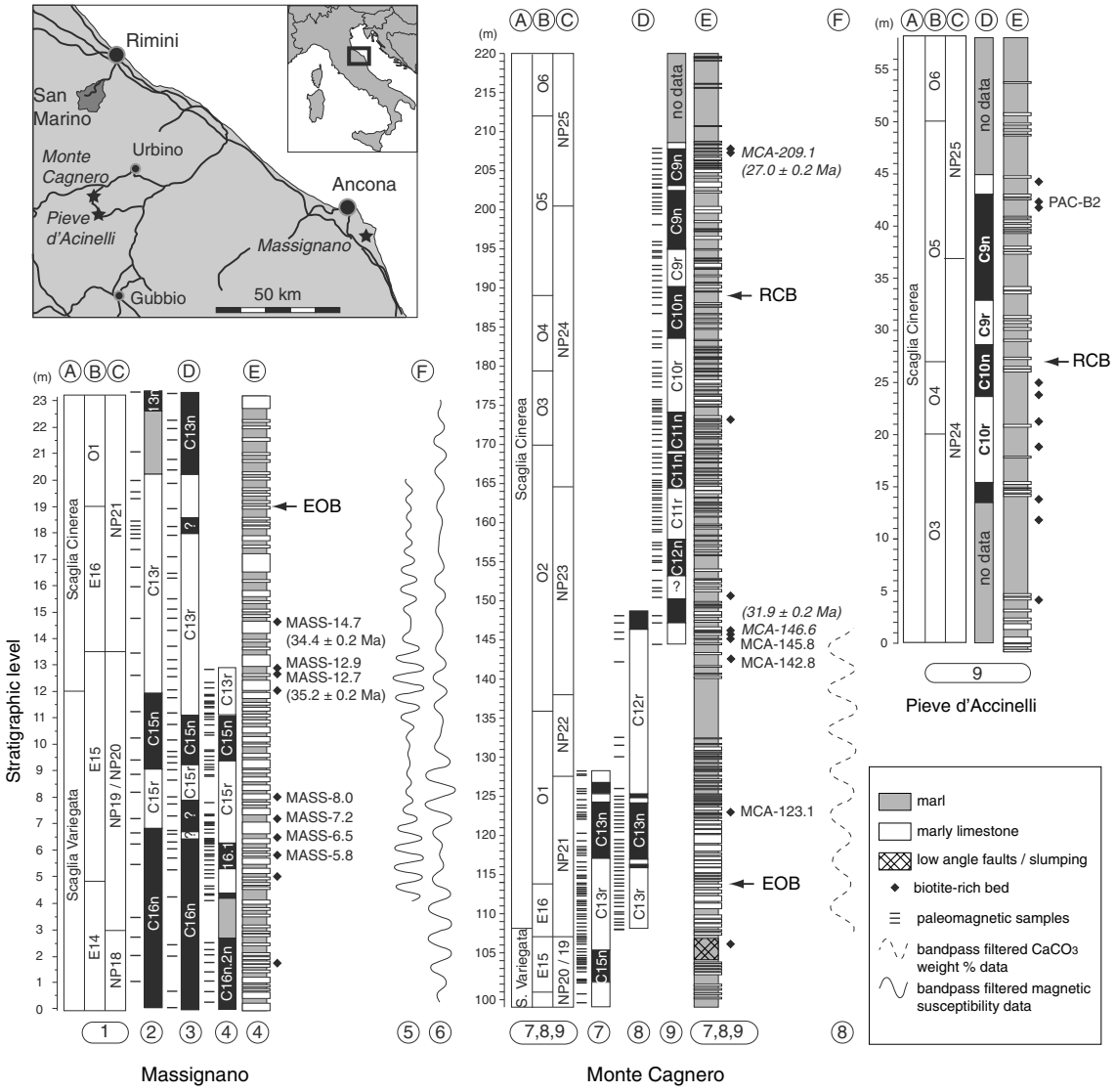

Figure 2. Late Eocene-Oligocene stratigraphic framework of the Umbria-Marche sedimentary record. Inset shows the location of the Massignano, Monte Cagnero, and Pieve d'Accinelli sections. A = lithostratigraphy, B = planktonic foraminifer biostratigraphy, C = calcareous nanoplankton biostratigraphy, D = magnetostratigraphy, E = lithology, F = astronomically tuned proxy records, 1 = Coccioni et al. (1988), 2 = Bice and Montanari (1988), 3 = Lowrie and Lanci (1994), 4 = Jovane et al. (2004), 5 = Jovane et al. (2006), 6 = Brown et al. (2009), 7 = Jovane et al. (2013), 8 = Hyland et al. (2009), 9 = Coccioni et al. (2008), EOB = Eocene-Oligocene boundary, RCB = Rupelian-Chattian boundary. Note that the vertical scale is different for each section. Band-pass-filtered proxy data used for astronomical tuning are plotted in the depth domain, with cycles interpreted as corresponding to the 100 kyr eccentricity signal at Massignano (Jovane et al., 2006; Brown et al., 2009) and the 405 kyr eccentricity signal at Monte Cagnero (ref. 8). Note that the two BRL listed in italics, MCA-146.6 and MCA-209.1, were not sampled for this study.

et al., 2015). The late Eocene portion of the ATPS06 (33.7–41 Ma) was not included in GTS12, because sediment accumulation below the carbonate compensation depth was thought to render the tuning unreliable (Pälike et al., 2006; Vandenberghe et al., 2012). Although a series of short (2–6 Ma) astronomically tuned time scales have been developed for the interval between 31.6 and 46.3 Ma (Brown et al., 2009; Hyland et al., 2009; Jovane et al., 2006, 2010; Pälike, Shackleton, & Röhl, 2001), at localities including Massignano and Monte Cagnero, which are thus directly tied to the $^{40}Ar/^{39}Ar$ data used to calibrate the RI-GPTS, gaps and discrepancies between these records also precluded their inclusion in the Paleogene AT-GPTS. Consequently, the AT-GPTS of GTS12 had to contend with a late Eocene gap (Figure 1) between the base of chron C13n (33.7 Ma; Pälike et al., 2006) and the base of chron C21n (47.8 Ma; Hilgen, Kuiper, & Lourens, 2010; Westerhold & Röhl, 2009). The latter chron boundary marks the younger end of a compilation of time scales tuned to the 405 kyr eccentricity component of the La2004 solution (Hilgen et al., 2010; Westerhold et al., 2007, 2008; Westerhold & Röhl, 2009), with a Cretaceous-

Paleogene boundary age of 65.95 Ma, consistent with $^{40}Ar/^{39}Ar$ dates bracketing the same boundary in Montana (Kuiper et al., 2008; Renne et al., 2013; Swisher et al., 1993). The late Eocene gap of GTS12 was bridged by sixth-order polynomial interpolation along the magnetic anomaly profile of Cande and Kent (1992). However, since the publication of GTS12, alternative astronomically tuned time scales covering the late Eocene gap have emerged from the tuning of the Pacific Equatorial Age Transect (PEAT (Westerhold et al., 2013); 30.9–41.3 Ma) and a series of deep-sea sites in the South Atlantic (Westerhold et al., 2015; 41–48 Ma).

This paper reevaluates the age of BRLs from the Umbria-Marche basin used to calibrate the RI-GPTS in GTS12 using high-precision zircon $^{206}Pb/^{238}U$ geochronology. The accuracy of the $^{206}Pb/^{238}U$ technique is underpinned by gravimetrically calibrated isotopic tracer solutions (Condon et al., 2015; McLean et al., 2015) and the determination of the ^{238}U decay constant through alpha counting experiments (Jaffey et al., 1971). Furthermore, the total uncertainties (i.e., including decay constant and tracer calibration uncertainties) of weighted mean $^{206}Pb/^{238}U$ dates are on the order of 0.12–0.2% (30 to 70 kyr for 25–35 Ma old samples) and are thus sufficiently low to constrain Milankovitch frequencies. Consequently, $^{206}Pb/^{238}U$ dating of the Umbria-Marche BRL facilitates an objective evaluation of the accuracy of both $^{40}Ar/^{39}Ar$ and cyclostratigraphic data sets from Massignano and Monte Cagnero. The aim is to examine potential causes of the Oligocene discrepancy between the RI-GPTS and AT-GPTS and to test the accuracy of the Oligocene portion of the AT-GPTS.

2. Geologic Setting and Published Geochronology

The Umbria-Marche basin in central Italy (Figure 2) hosts a near-continuous Triassic-Pliocene sedimentary succession that accumulated on the continental margin of the Adriatic promontory and underwent folding and thrusting during the Neogene closure of the Tethys Ocean (Alvarez & Montanari, 1988). The late Paleogene part of the record comprises rhythmic alternations of marl, marly limestone, and limestone deposited at a paleodepth of 1000–1500 m (Coccioni & Galeotti, 2003) and is subdivided into the Lutetian-Priabonian Scaglia Variegata formation and the Priabonian-Aquitanian Scaglia Cinerea formation. Both the Scaglia Variegata and the Scaglia Cinerea formations contain frequent centimeter-thick BRL (Montanari et al., 1988; Odin et al., 1991). Samples for this study were collected from three localities: Massignano, Monte Cagnero, and Pieve d'Accinelli. The lithostratigraphy, biostratigraphy, and magnetostratigraphy of these localities are summarized in Figure 2. All stratigraphic positions are reported in meters above the base of the respective sections.

2.1. Massignano

The Massignano section (43°32′09″N, 13°35′33″E; Figures 2 and 3) encompasses a 23 m thick late Eocene-early Oligocene record (approximately 35.8–33.5 Ma; Brown et al., 2009), and hosts the GSSP for the base of the Oligocene, defined by the last occurrence (LO) of hantkeninids at 19 m (Premoli Silva & Jenkins, 1993). The magnetic polarity pattern of the section correlates to chrons C16n.2n–C13n (Bice & Montanari, 1988; Jovane et al., 2007; Lowrie & Lanci, 1994). An array of low-precision (±0.2–1.0 Myr) K-Ar and Rb-Sr biotite dates and limited zircon and monazite U-Pb data have been published for BRL at 7.2, 12.7, 12.9, and 14.7 m (Montanari et al., 1985; Montanari et al., 1988; Oberli & Meier, 1991). Odin et al. (1991) reported $^{40}Ar/^{39}Ar$ plateau ages on multigrain biotite fractions from the BRL at 12.7 and 14.7 m (Figure 2). Astronomical tuning of the Massignano record resulted in two independent astronomically tuned time scales which estimate the age of the Eocene-Oligocene boundary (EOB) at 33.71 Ma (Jovane et al., 2006) and 33.91 ± 0.05 Ma, respectively (Brown et al., 2009).

2.2. Monte Cagnero

The Monte Cagnero section (43°38′50″N, 12°28′05″E; Figures 2 and 3) is located approximately 100 km northwest of Massignano, and spans 225 m, covering the late Eocene-Oligocene. This study focuses on the interval between 100 and 209 m (approximately 35.8–27.0 Ma; Coccioni et al., 2008; Jovane et al., 2013) and follows the revised stratigraphic framework of Coccioni et al. (2012). The LO of hantkeninids places the EOB at 114.1 m (Hyland et al., 2009), while the last common occurrence (LCO) of *Chiloguembelina cubensis* at 189 m marks a proposed GSSP for the base of the Chattian (Coccioni et al., 2008). The magnetic polarity record of the Monte Cagnero section is a composite of three partially overlapping and mutually consistent data sets and correlates to magnetochrons C18n–C8r (Coccioni et al., 2008; Hyland et al., 2009; Jovane

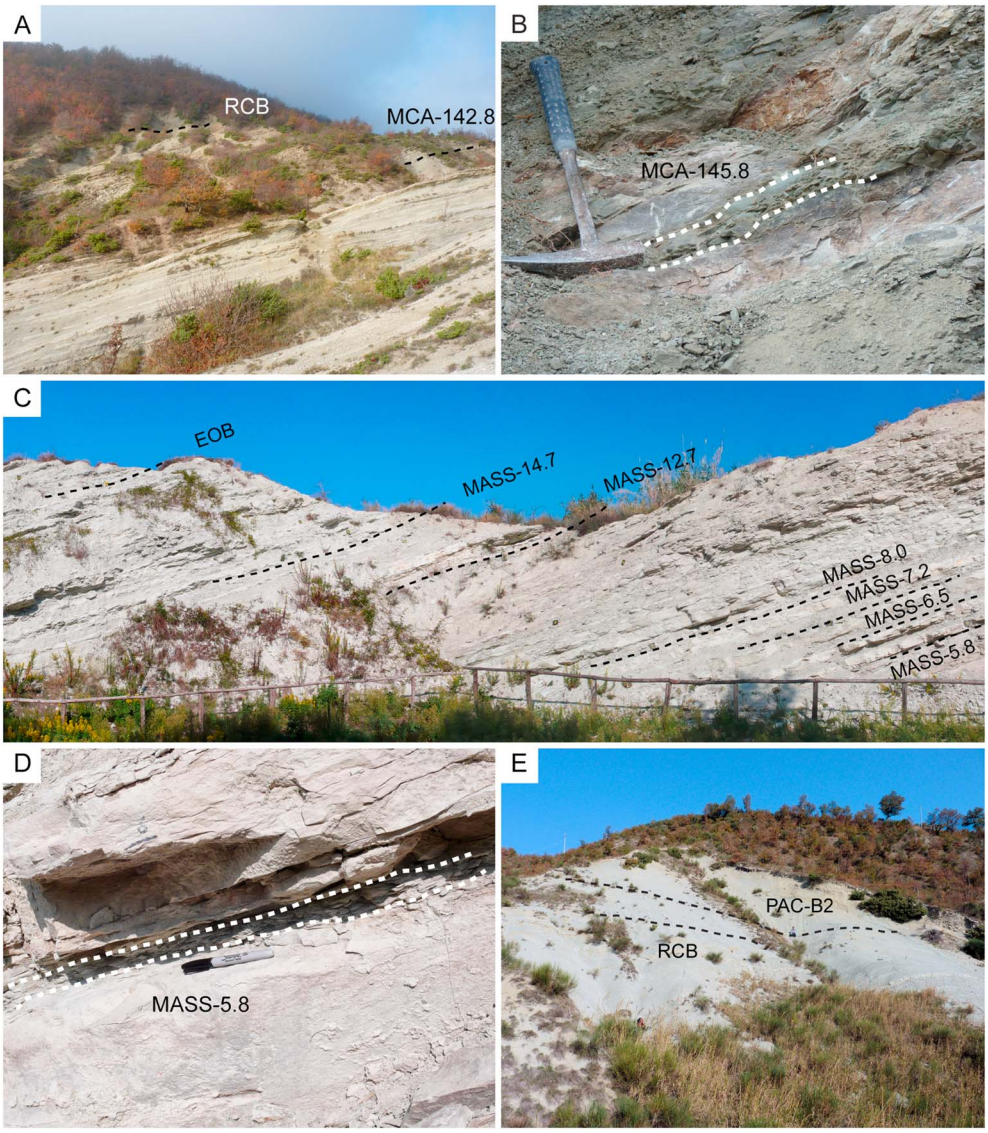

Figure 3. Overview of sampled outcrops: A = the Monte Cagnero section, with approximate locations of the Rupelian-Chattian boundary (RCB) and the biotite-rich layer (BRL) at 142.8 m; B = BRL at 145.8 m in the Monte Cagnero section; C = the Massignano section, with approximate locations of the Eocene-Oligocene boundary (EOB), and sampled BRL; D = BRL at 5.8 m in the Massignano section; E = the Pieve d'Accinelli section with approximate location of the B2 BRL (sample PAC-B2 in this study) and the RCB.

et al., 2013). Biotite from BRL at 146.6 m and 209.1 m has been dated at 31.9 ± 0.2 Ma and 27.0 ± 0.2 Ma, respectively (Coccioni et al., 2008), while astronomical tuning between 108 and 146 m resulted in an EOB age of 33.95 Ma (Hyland et al., 2009).

2.3. Pieve d'Accinelli

The Pieve d'Accinelli section (43°35′40″N, 12°29′34″E; Figure 2) is located approximately 1 km west of Piobbico and approximately 10 km southeast of Monte Cagnero. The LCO of *C. cubensis* places the base of the Chattian at 27 m, and the magnetic polarity pattern of the section between 13 and 46 m correlates to magnetochrons C11n.1n–C9n (Coccioni et al., 2008).

3. U-Pb Dating of Biotite-Rich Layers

We sampled 11 BRL from Massignano (n = 7), Monte Cagnero (n = 3), and Pieve d'Accinelli (n = 1). Zircons were separated from each sample using conventional mineral separation techniques. Eocene BRL from

Massignano typically had higher zircon yields compared to Oligocene BRL from Monte Cagnero and Pieve d'Accinelli. All samples contained mixed zircon populations with rounded grains and grain fragments (typically $<$150 μm in length), and euhedral grains with aspect ratios of 3–7 (100–200 μm in length), with the latter being the dominant population, and typical of zircon from volcanic ash (see Figure S1 in the supporting information). Cathodoluminescence imaging of representative euhedral zircons from two of the BRL sampled at Massignano (MASS-5.8 and MASS-7.2) indicated that lower aspect ratio grains frequently incorporate inherited xenocrystic cores (see Figure S2 in the supporting information) as is typical in volcanic rocks derived from crustal melts. Consequently, the selection of zircons for U-Pb dating focused on high aspect ratio crystals (complete crystals), and the tips of selected low aspect ratio grains in order to avoid xenocrystic cores and obtain data representative of the youngest zircon population from each sample. A total of 110 zircon and zircon fragments were dated using chemical abrasion isotope dilution thermal ionization mass spectrometry (CA-ID-TIMS) methodologies employed at the Natural Environment Research Council Isotope Geosciences Laboratory, British Geological Survey. Samples were processed using the analytical protocol outlined by Sahy et al. (2015); however, two pertinent points are briefly outlined here: (i) all zircons were chemically abraded (Mattinson, 2005) prior to dissolution in order minimize the effects of postcrystallization Pb loss and (ii) all zircons were spiked with the gravimetrically calibrated EARTHTIME ET535 (^{205}Pb-^{233}U-^{235}U) or ET2535 (^{202}Pb-^{205}Pb-^{233}U-^{235}U) isotopic tracer solutions (Condon et al., 2015; McLean et al., 2015), ensuring full traceability of the U-Pb results to SI units. Tabulated results are included in Table S2 in the supporting information.

Extracting reliable age information from volcanic tuff zircon data sets requires interpretation and the identification of predepositional and postdepositional biases (e.g., Schoene et al., 2013; Wotzlaw et al., 2013). Owing to the high closure temperature of zircon, each sample is likely to incorporate real age variation resulting from grains that crystallized at/close to the eruption and grains that crystallized prior to the eruption and give older apparent ^{206}Pb/^{238}U dates (i.e., antecrystic or xenocrystic zircon). The ^{206}Pb/^{238}U dates that postdate the eruption may result from minor postcrystallization Pb loss, which cannot be completely ruled out in spite of the use of chemical abrasion protocols. Pb loss in CA-ID-TIMS data typically manifests as one or more nonreproducible dates that are younger than the main zircon population thought to represent the eruption age and is expected to be a minor component, if present. Conversely, subtle inheritance, or prolonged crystallization, manifests as arrays of progressively older dates often spread out over several hundreds of kiloyears. Pb loss, inheritance, and prolonged crystallization are nonsystematic processes, affecting each grain to a different extent. For this reason our preferred interpretation of the data set relies on inverse variance-weighted mean ages based on at least three of the youngest single reproducible analyses as the best estimate of the eruption age of each sample.

Reproducibility is assessed at the 2σ level and is quantified through the mean square of the weighted deviates (MSWDs). Calculated MSWD values from this data set range between 0.29 and 1.58, within acceptable limits for weighted mean ages based on between four and seven analyses (Wendt & Carl, 1991), and are indicative of zircon populations that are free of geological scatter at the resolution of their respective analytical uncertainties (Figure 4 and Table 1; see section S1 in the supporting information for details on the selection of analyses included in our preferred weighted mean dates). Interpretations of the data set based on fewer analyses from the youngest population of each sample result in weighted mean ages that are statistically equivalent at the 2σ level to our preferred model (Table 1) and have no impact on the conclusions of this paper. Alternative interpretations that include additional data points compared to our preferred model result in unacceptably high MSWD values and are considered to have low probability (alternative interpretations of the U-Pb data are discussed in more detail in section S2 in the supporting information (Davydov et al., 2010; Dunn et al., 2012; Schoene et al., 2010; Meyers et al., 2012)). All interpreted weighted mean ^{206}Pb/^{238}U dates are consistent with the stratigraphic context of the samples, showing a clear upward younging trend at both Massignano and Monte Cagnero.

4. Numerical Age of the Umbria-Marche Succession

The ^{206}Pb/^{238}U dating of the Umbria-Marche BRL provides an opportunity to assess both published ^{40}Ar/^{39}Ar data used to calibrate the Eocene-Oligocene RI-GPTS in GTS12 and the astronomical time scales developed at Massignano and Monte Cagnero.

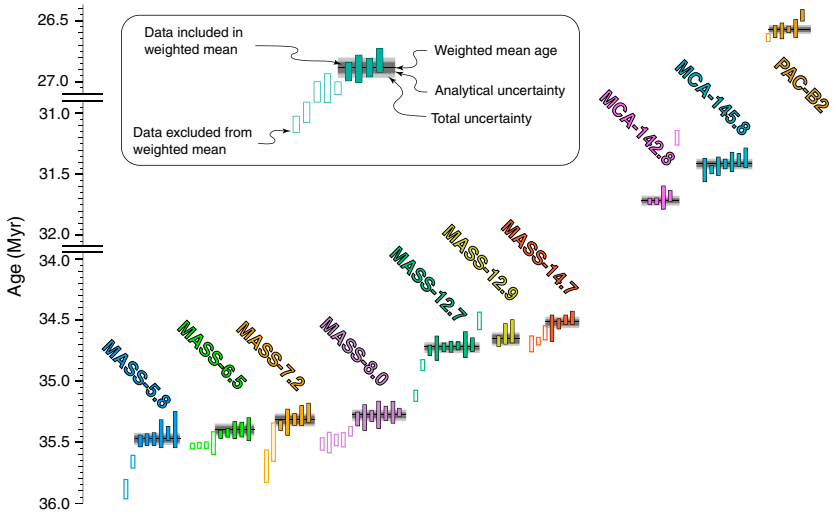

Figure 4. Plot of ranked $^{206}Pb/^{238}U$ dates from BRL from the Massignano, Monte Cagnero, and Pieve d'Accinelli sections. The total uncertainty of each weighted mean age includes the ^{238}U decay constant uncertainty and EARTHTIME U-Pb tracer calibration uncertainty. Note that the vertical time axis is not continuous.

4.1. Implications for Published $^{40}Ar/^{39}Ar$ Dates From Massignano and Monte Cagnero

At Massignano, Odin et al. (1991) published $^{40}Ar/^{39}Ar$ dates from two of the BRLs dated in this study: MASS-12.7 and MASS-14.7. Additionally, two of our samples fall stratigraphically close to previously dated BRL from Monte Cagnero: (i) MCA-145.8 which is situated 80 cm below a $^{40}Ar/^{39}Ar$-dated BRL at 146.6 m and (ii) sample PAC-B2 from Pieve d'Accinelli, identified in the field based on Figure 6b of Coccioni et al. (2008), which falls close to the top of C9n (C9n(.96)) and is therefore likely equivalent to one of the $^{40}Ar/^{39}Ar$ dated BRL situated at 208.7 (C9n(.94)) and 209.1 m (C9n(.98)), respectively, at Monte Cagnero (Coccioni et al., 2008). Mean sediment accumulation rates for the middle and upper parts of the Monte Cagnero record are approximately 10.4 and 13 m/Myr, respectively, based on our U-Pb data (Figure 5). Consequently, the time elapsed between the deposition of BRL pairs at 145.8–146.6 m (approximately 80 kyr) and 208.7–209.1 m (approximately 50 kyr) is less than the 100–200 kyr uncertainty of the $^{40}Ar/^{39}Ar$ dates of Coccioni et al. (2008), and $^{206}Pb/^{238}U$ and $^{40}Ar/^{39}Ar$ data pairs from these closely spaced BRL should be statistically equivalent at the 2σ level, assuming that both isotope systems are giving accurate dates. However, at both Massignano and Monte Cagnero, calibration relative to an FCs age of 28.201 Ma (Kuiper et al., 2008) adopted in GTS12 (Schmitz, 2012) results in

Table 1
Weighted Mean $^{206}Pb/^{238}U$ Ages of BRL From the Umbria-Marche Sedimentary Succession

Sample	IGSN	$^{206}Pb/^{238}U$ date	Uncertainty (2σ)	MSWD	*n*
PAC-B2	IEDS10014	26.573	±0.019/0.021/0.035	0.29	5 of 7
MCA-145.8	IEDS10013	31.407	±0.022/0.027/0.043	0.70	6 of 7
MCA-142.8	IEDS10012	31.716	±0.017/0.022/0.041	0.45	4 of 5
MCA-123.1	IEDS10011	33.291	±0.057/0.059/0.069	-	1 of 5
MASS-14.7	IEDS10010	34.497	±0.031/0.035/0.051	0.49	3 of 7
MASS-12.9	IEDS1000Z	34.681	±0.037/0.040/0.055	1.58	3 of 3
MASS-12.7	IEDS1000Y	34.720	±0.017/0.024/0.044	0.41	7 of 10
MASS-8.0	IEDS1000X	35.276	±0.019/0.025/0.045	0.93	7 of 12
MASS-7.2	IEDS1000W	35.340	±0.026/0.030/0.048	1.05	5 of 7
MASS-6.5	IEDS1000V	35.401	±0.019/0.025/0.045	1.09	6 of 10
MASS-5.8	IEDS1000U	35.467	±0.025/0.031/0.049	0.86	6 of 9

Note. MSWD = mean square of the weighted deviates, *n* = number of grains included in each weighted mean date out of the total number of grains analyzed (after rejection of discordant analyses and those with Pb*/Pbc < 1; see section S1 in the supporting information). Weighted mean dates and propagated uncertainties were calculated using the Tripoli and Redux U-Pb data reduction software packages (Bowring, McLean, & Bowring, 2011; McLean, Bowring, & Bowring, 2011). Uncertainties are quoted as ±*x*/*y*/*z*, where *x* denotes analytical uncertainty, while *y* and *z* indicated additional propagated systematic uncertainties related to the calibration of the EARTHTIME isotopic tracers and the ^{238}U decay constant.

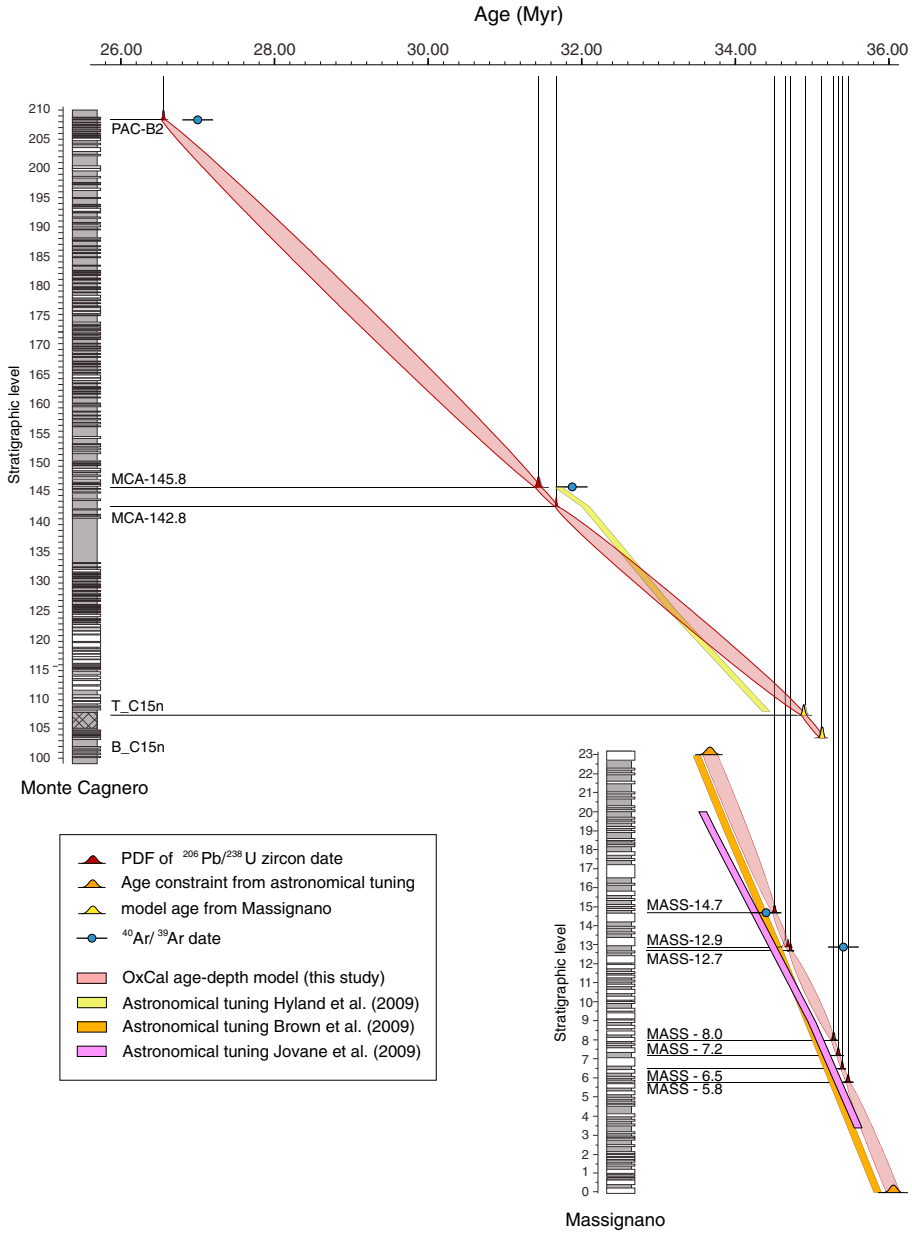

Figure 5. Comparison between $^{206}Pb/^{238}U$-calibrated age-depth models from this study and published $^{40}Ar/^{39}Ar$ dating and astronomical tuning of the Massignano and Monte Cagnero records. PDF = modeled probability density function. Note that the dates for the top and base of chron C15n, which are used to anchor the older end of the Monte Cagnero age-depth model, are output from the Massignano age-depth model developed in this study (see section S3 in the supporting information for details).

$^{40}Ar/^{39}Ar$ dates that are 0.4–0.5 Myr older than $^{206}Pb/^{238}U$ data from this study except for sample MASS-14.7, for which $^{206}Pb/^{238}U$ and recalculated $^{40}Ar/^{39}Ar$ dates are equivalent (Figure 5). A FCs age of 28.2 Ma with an uncertainty of less than ±0.1 Ma is supported by multiple independent attempts to calibrate $^{40}Ar/^{39}Ar$ mineral standards against astronomically tuned records (Kuiper et al., 2008; Rivera et al., 2011), and input from the $^{206}Pb/^{238}U$ system and other primary measurements (Renne et al., 2010), as well as U-Pb (zircon) dating of the Fish Canyon tuff (Wotzlaw et al., 2013) and paired $^{40}Ar/^{39}Ar$ and $^{206}Pb/^{238}U$ data from Eocene and Cretaceous successions in North America (Renne et al., 2013; Sageman et al., 2014). While an FCs age of 28.0 Ma or less would result in better agreement between $^{206}Pb/^{238}U$ and $^{40}Ar/^{39}Ar$ pairs from the Umbria-Marche record, studies advocating such young FCs ages (e.g., Channell et al., 2010) have been refuted

(Singer, 2014). Since the discrepancy between $^{206}Pb/^{238}U$ and $^{40}Ar/^{39}Ar$ dates from Massignano and Monte Cagnero is not systematic, other processes, capable of biasing individual zircon and or biotite dates, must have been active. Anomalously young zircon $^{206}Pb/^{238}U$ dates may result from postcrystallization Pb loss; however, this has been mitigated through chemical abrasion protocols (Mattinson, 2005) and the use of multiple reproducible analyses with no detectable geological scatter to calculate each weighted mean age. The accuracy of our weighted mean $^{206}Pb/^{238}U$ dates is further supported by the clear upward younging trend observed in the lower part of the Massignano record, where the time elapsed between the deposition of consecutive BRL is comparable to the uncertainties of the individual weighted mean dates. Conversely, anomalously old biotite $^{40}Ar/^{39}Ar$ dates may result from ^{39}Ar recoil due to neutron irradiation (Paine, Nomade, & Renne, 2006) and/or the presence of initial ^{40}Ar which has been demonstrated to generate discrepancies of up to 600 kyr between $^{40}Ar/^{39}Ar$ dates from coeval biotite and sanidine (Hora et al., 2010). Additionally, subtle variations in the age and excess ^{40}Ar systematics of individual biotite crystals would have been masked by the analysis of multigrain fractions at both Massignano and Monte Cagnero (Coccioni et al., 2008; Odin et al., 1991). Furthermore, the $^{40}Ar/^{39}Ar$ dates for samples MASS-12.7 and MASS-14.7 were originally reported relative to LP-6 biotite, which is itself known to be heterogeneous (Spell & McDougall, 2003). Consequently, our interpretation is that three of the four published $^{40}Ar/^{39}Ar$ dates from Massignano and Monte Cagnero are anomalously old, and we attribute this to a combination of factors related to the geological complexity of the analyzed biotite samples and/or mineral standards.

4.2. Implications for the Astronomically Tuned Massignano and Monte Cagnero Records

The astronomical time scales developed at Massignano and Monte Cagnero provide continuous age information for the respective records at the resolution of the 40 kyr obliquity (Jovane et al., 2006) and 100 kyr eccentricity cycles (Brown et al., 2009; Hyland et al., 2009) of the La2004 model, based on carbonate concentration and magnetic susceptibility proxy records. Assuming that cycle expression and identification is complete and accurate, estimates of the time elapsed between the deposition of consecutive BRL should have a precision comparable to that of the $^{206}Pb/^{238}U$ method (±20–50 kyr). It should be noted that the precise age interpretation of Eocene obliquity cycles, which were used to fine-tune the interpretation of marl/limestone alternations at Massignano by Jovane et al. (2006), is problematic, given the impact of tidal dissipation; however, the frequency of the obliquity signal can be considered constant over the time spanned by the Massignano record.

At Massignano, two partially overlapping orbital chronologies estimate the duration of the interval between 4 and 20 m at 2.1 Myr (Jovane et al., 2006) and 1.6 Myr (Brown et al., 2009), respectively. Weighted mean $^{206}Pb/^{238}U$ dates from Massignano are older than both astronomically tuned age models (Figure 5). The discrepancy relative to the tuning of Jovane et al. (2006) increases linearly from approximately 100 to 300 kyr between 5.8 m and 14.7 m. Conversely, the tuning of Brown et al. (2009) is in good agreement with our results in relative terms (i.e., the astronomically tuned and radio-isotopically calibrated durations of intervals bracketed by U-Pb dated BRL are equivalent), but absolute ages derived from the tuned record are approximately 200 kyr younger than those based on $^{206}Pb/^{238}U$ dating. Jovane et al. (2006) based their initial tuning on matching cycles with periods of 72 and 284 cm in the depth domain to the 100 and 405 kyr eccentricity signals assuming a mean sediment accumulation rate of approximately 7 m/Myr based on the RI-GPTS of Cande and Kent (1995). However, $^{206}Pb/^{238}U$ data from this study indicate that mean sediment accumulation rates at Massignano were slightly higher, at approximately 9.5 m/Myr, which implies that periodicities of 72 and 284 cm in the depth domain translate into approximately 70 and 300 kyr, respectively, in the time domain. Spectral analysis of $CaCO_3$ weight percent and magnetic susceptibility data from the entire Massignano section (0.5–23 m) carried out by Brown et al. (2009), who assumed a sediment accumulation rate of 10.6 m/Myr, also revealed statistically significant (at the 95% confidence level) peaks around 315 and 66 kyr; however, these became less prominent when data from the lower (0.5–15 m) and upper (15–23 m) portions of the section were analyzed separately and are therefore likely to be statistical artifacts (see Figures 4–6 of Brown et al., 2009). The implication is that, based on the mean sediment accumulation rate derived from the $^{206}Pb/^{238}U$ date BRL, the discrepancy between the two orbital time scales developed at Massignano appears to stem from an error in the identification of long and short eccentricity cycles in the tuning of Jovane et al. (2006). However, this does not explain the 200 kyr offset between the tuning of Brown et al. (2009) and this study.

At Monte Cagnero, the tuning of $CaCO_3$ weight percent data between 108 and 146 m to the La2004 numerical solution (Hyland et al., 2009) is anchored by a 31.5 ± 0.2 Ma $^{40}Ar/^{39}Ar$ date from a BRL at 146.6 m (Coccioni et al., 2008; reported relative to FCs = 27.84 Ma). This date increases to 31.8 ± 0.2 Ma when recalculated relative to FCs = 28.201 Ma, which is approximately 400 kyr older than the $^{206}Pb/^{238}U$ date from sample MCA-145.8 (0.8 m lower in the record, 31.41 ± 0.04 Ma) and statistically equivalent to the $^{206}Pb/^{238}U$ date from sample MCA-142.8 (3.8 m lower in the record, 31.72 ± 0.04 Ma). Given that $^{206}Pb/^{238}U$ dating indicates a mean sediment accumulation rate of approximately 10 m/Myr, the implication is that the tuning of the Monte Cagnero record may be offset by one 405 kyr eccentricity cycle. However, simply shifting the tuning of Hyland et al. (2009) forward by one 405 kyr cycle results in an EOB age of 33.55 Ma, significantly younger than reported in the ATPS06 and PEAT records (Pälike et al., 2006; Westerhold et al., 2013). Furthermore, such a shift in the Monte Cagnero tuning would also result in an age of approximately 34.0 Ma for the older end of the tuned record at 108 m, which in conjunction with the position of the top of magnetochron C15n at 106.1 m (Jovane et al., 2013), dated at 35.13 Ma in the ATPS06, would indicate either a drop in sediment accumulation rates from 10 m/Myr to approximately 1.7 m/Myr or a approximately 800 kyr hiatus. However, both of these options seem unlikely, given that the duration of planktonic foraminifer biozones E15 and E16 which bracket the 108–106.1 m interval (approximately 600 kyr, each assuming a sediment accumulation rate of 10 m/Myr) are similar to those calculated at Massignano (680 kyr and 630 kyr, respectively) and reported elsewhere (Wade et al., 2011; approximately 700 kyr each relative to ATPS06). Consequently, U-Pb data from this study indicate possible errors in both the absolute timing and relative chronology of the astronomical tuning of the Monte Cagnero record. A possible explanation would be that a 405 kyr cycle has been overlooked in the cyclostratigraphic interpretation of the $CaCO_3$ record of Monte Cagnero.

4.3. Age-Depth Models

Revised age-depth models for the Massignano and Monte Cagnero records were developed using the Bayesian approach implemented in the P_Sequence routine of the OxCal 4.2 software package (Bronk Ramsey, 2008). Briefly, the model treats sediment accumulation as a random Poisson process, in which layers of finite thickness are deposited at discrete points in time and are separated by gaps of variable duration (Bronk Ramsey, 2008). Additionally, OxCal has the flexibility to integrate radio-isotopic age constraints with other type of information, such as relative chronologies built upon astronomical tuning and, where available, other stratigraphic information. While this flexibility is one of OxCal's greatest strengths, it is also, potentially, its greatest weakness, because it allows the user a certain amount of control over the trajectory of the output age-depth model and the width of its uncertainty envelope. The main factors through which this control is exerted are the selection of priors (i.e., the manner in which the available data are fed into the software) and the stratigraphic resolution of the model. Priors for the age-depth models developed in this study consist of $^{206}Pb/^{238}U$ dates and their uncertainties for both the Massignano and Monte Cagnero records. The Massignano model further includes a relative chronology built upon the astronomically tuned record of Brown et al. (2009) as the sediment accumulation rates between levels 5.8 m and 14.7 m are concordant with those derived from the U-Pb (zircon) data. This approach results in improved precision between 5.8 and 14.7 m (±15–35 kyr versus ±20–70 kyr based on $^{206}Pb/^{238}U$ data alone, excluding systematic U-Pb uncertainties) and eliminates the need for extrapolation in order to date events outside the 5.8–14.7 m interval (e.g., the EOB). The durations of astronomically tuned intervals included in the model and their uncertainties are summarized in section S3.1 and Table S1 in the supporting information. The age-depth model developed at Monte Cagnero (Figure 5) is based on $^{206}Pb/^{238}U$ data from samples MCA-142.8, MCA-145.8, and PAC-B2 with the latter correlated to the BRL at 209.1 m. The tuning of Hyland et al. (2009) was not included in the age-depth model due to inconsistencies relative to the $^{206}Pb/^{238}U$ data set (see section 4.2). Instead, the lower end of the Monte Cagnero record is anchored by the modeled age of the top and base of C15n at Massignano. OxCal treats radio-isotopic date uncertainties as random, which means that when correlated systematic uncertainties are present, the resulting age model will have an unrealistically narrow uncertainty envelope for stratigraphic intervals with closely spaced $^{206}Pb/^{238}U$ dates with overlapping uncertainties. For this reason, only the analytical uncertainties of weighted mean $^{206}Pb/^{238}U$ dates were modeled in OxCal and additional systematic uncertainties equivalent to ±0.03% and 0.11% of the interpolated ages, representing U-Pb tracer calibration and ^{238}U decay constant uncertainties at the 2σ level, were added in quadrature to the 95% uncertainty envelope of the age model. The stratigraphic resolution of the model is defined by the user-specified *k* value, which signifies the number of depositional events expected to occur per unit dept, and

Table 2
Interpolated Age of Magnetic Reversals and Planktonic Foraminifera Bioevents Recorded in the Massignano and Monte Cagnero Sections

	Monte Cagnero		Massignano	
	Meter level	Age ± 2σ (Myr)	Meter level	Age ± 2σ (Myr)
Base C8r*	209.4	26.60 ± 0.07		
Base C9n	196.0	27.58 ± 0.15		
Base C9r	191.3	27.94 ± 0.17		
LCO *Chiloguembelina cubensis*	189.0	28.11 ± 0.17		
Base C10n	184.4	28.46 ± 0.18		
LO *Globigerina angulisuturalis*	179.0	28.88 ± 0.19		
Base C10r	175.0	29.18 ± 0.19		
LO *Turborotalia ampliapertura*	170.0	29.56 ± 0.18		
Base C11n	165.4	29.91 ± 0.17		
FO *Globigerinatheca ciperoensis*	165.0	29.94 ± 0.17		
LO *Subbotina angiporoides*	161.5	30.21 ± 0.16		
Base C11r	158.9	30.41 ± 0.15		
Base C12n	148.2	31.23 ± 0.08		
LO *Isthmolithus recurvus*	139.0	32.00 ± 0.09		
LO *Pseudohastigerina naguewichiensis*	137.0	32.15 ± 0.10		
Base C12r	124.2	33.09 ± 0.07		
Oi-1	118.0	33.69 ± 0.13		
Base C13n	117.3	33.74 ± 0.13	20.2	33.97 ± 0.08
LO Hantkeninidae	114.1	34.08 ± 0.13	19.0	34.09 ± 0.08
LO *Turborotalia cerroazulensis*	113.6	34.14 ± 0.13		
LO *Cribohantkenina inflata*	112.9	34.20 ± 0.13	15.0	34.48 ± 0.05
LO *Globigerinatheka index*	107.5	34.75 ± 0.08	13.5	34.63 ± 0.05
LO *Turborotalia cunialensis*	102.5	35.11 ± 0.05	18.6	34.13 ± 0.08
LO *Turborotalia cocoanensis*			18.6	34.13 ± 0.08
LO *Globigerinatheka luterbacheri*			12.9	34.70 ± 0.04
Base C13r	106.1		11.1	34.91 ± 0.07
Base C15n	102.3		9.3	35.11 ± 0.07
FO *Turborotalia cunialensis*			7.5	35.31 ± 0.05
Base C15r			6.2	35.43 ± 0.05
FO *Cribohantkenina inflata*			5.8	35.47 ± 0.05
Base C16n.1n			5.5	35.50 ± 0.05
LO *Turborotalia pomeroli*			5.0	35.54 ± 0.06
LO *Globigerinatheka semiinvoluta*			4.8	35.55 ± 0.06
Base C16n.1r			3.3	35.68 ± 0.07

Note. Biostratigraphy and magnetostratigraphy of the Massignano section is based on Coccioni et al. (1988), Bice and Montanari (1988), and Jovane et al. (2007). Biostratigraphy and magnetostratigraphy of the Monte Cagnero section is based on Coccioni et al. (2008), Hyland et al. (2009), and Jovane et al. (2013). Uncertainties include propagated U-Pb tracer calibration and ^{238}U decay constant uncertainty. The higher uncertainty of the Monte Cagnero age-depth model (compared to Massignano) reflects the wide stratigraphic spacing of the dated BRL. Asterisk indicates the age based on linear extrapolation using a modeled mean apparent sediment accumulation rate of 13 m/Myr between BRL at 145.8 m and 209.1 m at Monte Cagnero.

must be appropriate for the nature of the modeled sedimentary succession. Because the Umbria-Marche succession consists of fine-grained pelagic sediments, we selected an initial *k* value of 1000 with a uniform probability density function covering 2 orders of magnitude in either direction—this is equivalent to 10^1–10^5 depositional events per meter depth. The impact of the *k* value, and specifically its probability density function, on the trajectory and uncertainty envelope of the Monte Cagnero age-depth model is discussed in section S3.2 in the supporting information. It should be noted however that higher *k* values limit the degree to which sediment accumulation rates can vary within the model. This is relevant for the upper portion of the Monte Cagnero model between the MCA145.8 and PAC-B2 BRL, as changes in sediment accumulation rates within this approximately 5 Ma interval cannot be accounted for in the absence of additional age information. Bearing in mind the above caveats, OxCal age-depth models are expected to produce output data that are correct for 95% of the possible scenarios described by the input data (Bronk Ramsey, 2000). Details of the two age-depth models along with output data for the Massignano and Monte Cagnero records, at a resolution of 10 cm, are included in section S3 and Tables S3 and S4 in the supporting information (Blaauw & Christen, 2005; Christen & Perez, 2009; Hercman & Pawlak, 2012; Scholz & Hoffmann, 2011; Machlus et al., 2004; Mundil et al., 2004; Smith et al., 2010; Zanazzi et al., 2007). Modeled ages for magnetic reversals and key planktonic foraminifer bioevents recorded at Massignano and Monte Cagnero are summarized in Table 2.

5. Discussion

5.1. The Numerical Age of the Eocene-Oligocene Boundary

The GSSP of the EOB is defined by the LO of the planktonic foraminifer genus Hantkenina, 19 m above the base of the Massignano section (Premoli Silva & Jenkins, 1993). The LO of hantkeninids has been astronomically dated to 33.90 ± 0.05 Ma at Massignano (Brown et al., 2009). Alternative tuning options for the EOB interval in the Umbria-Marche basin are not discussed here, because the $^{206}Pb/^{238}U$ data presented in this paper indicate possible errors in the identification of long/short eccentricity cycles in the relevant proxy records (see section 4.2 for details). We report statistically equivalent modeled EOB ages from Massignano (34.09 ± 0.08 Ma) and Monte Cagnero (34.08 ± 0.13 Ma). Note that these dates are not independent of each other, because the older end of our age-depth model for the Monte Cagnero record is anchored by data extracted from the age-depth model developed for the Massignano record in this study (see section S3 in the supporting information). However, agreement between the two modeled EOB dates does confirm that the time elapsed between the beginning of chron C13r and the LO of hantkeninids is consistent between the Massignano and Monte Cagnero records. These modeled dates are nominally approximately 190 kyr older than the 33.90 Ma EOB age extracted from the tuning of the Massignano record, which reflects the approximately 200 kyr offset between zircon U-Pb-based age model and the tuning of Brown et al. (2009) throughout the section (see section 4.2 for details). Our modeled dates are also older than EOB ages reported from the

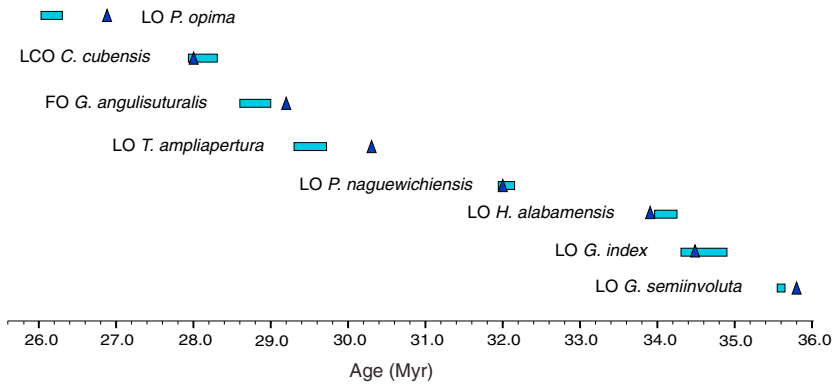

Figure 6. Timing of planktonic foraminifer bioevents reported from Massignano and Monte Cagnero (blue bars; data from Table 2) based on our age model and the revised tropical/subtropical planktonic foraminifer biozonation scheme of Wade et al. (2011) (blue triangles) calibrated relative to the ATPS06.

ATPS06 (33.79 Ma; Pälike et al., 2006) and the PEAT record (33.89 Ma; Westerhold et al., 2013). However, neither the ATPS06 nor PEAT time scales directly date the LO of hantkeninids but rely instead on a magnetostratigraphic proxy for the EOB placed at C13r(.14) (Premoli Silva & Jenkins, 1993) based on the magnetic polarity pattern of Bice and Montanari (1988), who reported that the base of C13n is located at 20.2 m in the Massignano section. This magnetostratigraphic calibration of the EOB conflicts with subsequent work carried out at Massignano, which places the base of C13n higher in the section, between 21 and 22.5 m (Lowrie & Lanci, 1994). This is in line with other late Eocene-early Oligocene outcrops from the Umbria-Marche basin, where the LO of hantkeninids has been reported between C13r(.27) and C13r(.36) (Lanci, Lowrie, & Montanari, 1996). At Monte Cagnero, where the extent of chron C13r is constrained by two overlapping and mutually consistent paleomagnetic data sets (Jovane et al., 2013; Hyland et al., 2009) (see Figure 2), the LO of hantkeninids (114.1 m) falls at C13r(.28), while a theoretical point situated at C13r(.14) corresponding to the EOB as used in the ATS06 and PEAT tuning would fall at 115.7 m (Hyland et al., 2009; Jovane et al., 2013), with a modeled age of 33.92 ± 0.13 Ma, statistically equivalent to the EOB ages reported from both the PEAT record and the ATPS06.

5.2. The Age of the Rupelian-Chattian Boundary

The LCO of *C. cubensis* at 189 m in the Monte Cagnero section has been proposed as a site for the GSSP of the Chattian (Coccioni et al., 2008). However, Van Simaeys et al. (2004) argued against the use of the *Chiloguembelina* criterion for the Rupelian-Chattian boundary (RCB), on the grounds of diachroneity between the western Tethys and open ocean settings. Some planktonic foraminifer events recorded at Monte Cagnero do indeed appear to postdate their reported occurrence in open ocean settings (Figure 6). Notable examples are the LO of *Turborotalia ampliapertura* at the base of zone O_3 and the first occurrence of *Globigerina angulisuturalis*, at the base of zone O_4 which appear to be 400 and 200 kyr younger, respectively, than reported in a review of planktonic foraminifer biozonation relative to the ATPS06 by Wade et al. (2011). While these offsets could be at least partially attributed to poor preservation and/or the sampling resolution of the Monte Cagnero record, their interpretation as genuinely diachronous events is supported by mutually consistent magnetostratigraphic calibrations in the Monte Cagnero, Contessa Barbetti, and Pieve d'Accinelli records (Coccioni et al., 2008). This however is not the case for the LCO of *C. cubensis*, which has been consistently associated with chron C10n in the Umbria-Marche basin (Coccioni et al., 2008); ODP Site 1218 (Wade, Berggren, & Olsson, 2007); and DSDP Sites 516, 558, and 529 (Hess et al., 1989; Miller et al., 1985; Pujol, 1983), while sporadic Chattian occurrences of chiloguembelinids at DSDP Site 522 and ODP Sites 628 and 803 have been attributed to reworking (Leckie, Farnham, & Schmidt, 1993; Poore et al., 1983). Our modeled age for the LCO of *C. cubensis* at 189 m in the Monte Cagnero section is 28.11 ± 0.17 Ma, in agreement with the astronomically tuned estimate of 28.0 Ma of Wade et al. (2011) based on the ATPS06.

5.3. The Late Eocene-Oligocene Astronomical and Radio-Isotopic Time Scale Disparity

Magnetic reversal ages derived in the RI-GPTS of GTS12 (Vandenberghe et al., 2012), although recalculated relative to an FCs age of 28.201 Ma, are on average 0.5 Myr older than interpolated magnetic reversal ages

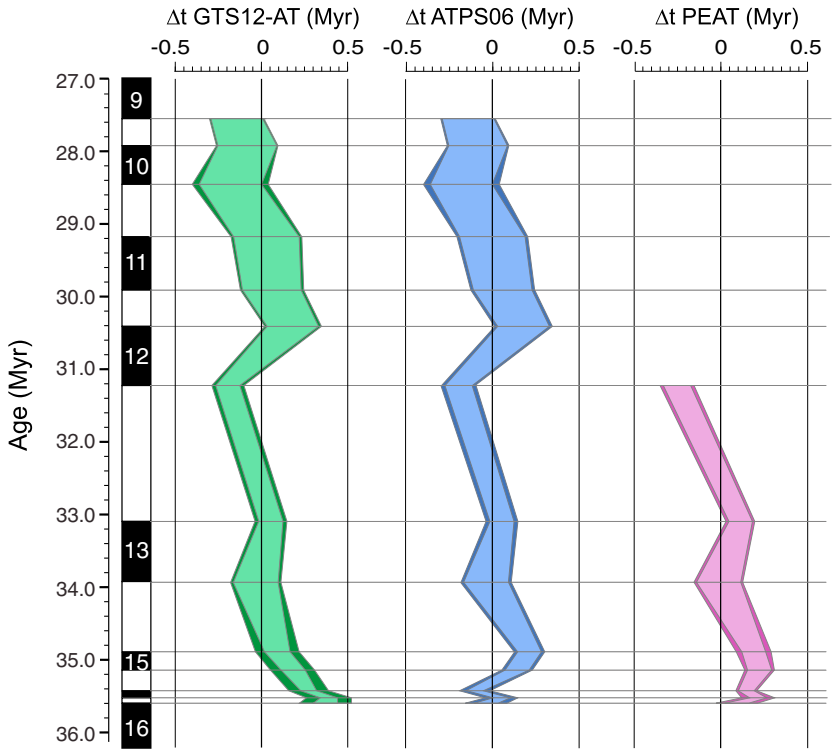

Figure 7. Comparison between modeled magnetic reversal ages from Massignano and Monte Cagnero (this study) and published astronomically tuned geomagnetic polarity time scales. Uncertainty envelopes encompass the total uncertainty of the $^{206}Pb/^{238}U$-calibrated age models developed in this study (lighter shade), with darker shaded envelope representing the impact of stratigraphic uncertainty in the placement of magnetic reversals at Massignano and Monte Cagnero (see section S4 and Table S5 in the supporting information for details), a ±0.1% systematic uncertainty for the La2004 numerical solution and, depending on the choice of time scale, a ±100 kyr uncertainty on the interpolated late Eocene option of the GTS12-AT, a ±40 kyr uncertainty on the ATPS06, or the magnetic reversal age uncertainties quoted by Westerhold et al. (2013) for the PEAT record (the latter were assumed to be quoted at the 1σ level), added in quadrature. Positive (negative) values indicate that $^{206}Pb/^{238}U$ calibrated reversal ages from this study are younger (older) than the respective GPTS. Note that chrons C10n.1r and C11n.1r which were identified based on single reversed polarity samples at Monte Cagnero (Coccioni et al., 2008) are not plotted.

from this study. We attribute this discrepancy to the use of anomalously old biotite $^{40}Ar/^{39}Ar$ dates from the Umbria-Marche basin in GTS12 (see section 4.1). This assertion is supported by the good agreement between modeled Oligocene magnetic reversal ages from Monte Cagnero and the ATPS06, which also underpins the AT-GPTS between 23 and 34 Ma (Figure 7). The only inconsistency appears to be the age for the base of chron C12n. However, the identification of this particular chron boundary in the Monte Cagnero record is somewhat ambiguous and was reported at 148.2 m by Coccioni et al. (2008) and approximately 146.5 m by Hyland et al. (2009). While this essentially resolves the Oligocene discrepancy reported between the RI-GPTS and AT-GPTS of GTS12, some inconsistencies persist between $^{206}Pb/^{238}U$-calibrated late Eocene magnetic reversal ages from Massignano and astronomically tuned AT-GPTS, ATPS06, and PEAT records (Figure 7). Late Eocene magnetic reversal ages from the AT-GPTS of GTS12 are 100–400 kyr older than those calculated in this study. Between 34 and 47 Ma (Figure 7), the AT-GPTS relies on sixth-order polynomial interpolation along the marine anomaly profile of Cande and Kent (1992), using astronomically tuned ages for the base of C13n (33.71 Ma; ATPS06) and C21n (47.8 Ma; Westerhold & Röhl, 2009) as tie points (Vandenberghe et al., 2012). The date derived for the base of C13n at Monte Cagnero is approximately 200 kyr older than that listed in the ATPS06. However, at Massignano the age of the same chron boundary could vary between 33.97 ± 0.08 and 33.75 ± 0.06, dependent upon a choice between the magnetic polarity records of Bice and Montanari (1988) and Lowrie and Lanci (1994), with the latter option indistinguishable from the ATPS06 age. The age used in GTS12 for the base of C21n is based on the tuning of ODP Site 1258 (Westerhold & Röhl, 2009) and marks the younger end of

the Paleocene-middle Eocene astronomical time scale (Hilgen et al., 2010; Westerhold et al., 2007, 2008; Westerhold & Röhl, 2009).

Vandenberghe et al. (2012) noted that the relative durations of magnetochrons C23n.2n and C23n (1:1) at ODP Site 1258 are not consistent with the magnetic anomaly profile of Cande and Kent (1992) (1:2), which implies the possibility of a 400–500 kyr hiatus, or an error in the tuning of the ODP Site 1258 record to the 405 kyr cycle or uncertainty in the marine anomaly profile. Consequently, these discrepancies between different time scales (Figure 7) may result from inaccuracies in the marine anomaly profile of Cande and Kent (1992), an artefact of the interpolation method chosen in GTS12, the astronomically tuned tie points, uncertainty in position of chron boundaries within stratigraphic age model, and a combination of the above factors.

The late Eocene portion of the ATPS06 has nonsystematic discrepancies of up to 200 kyr, particularly at the level of chron C15n when compared to the U-Pb (zircon)-based age model (this study). Conversely, magnetic reversal ages extracted from the PEAT record are approximately 150 kyr older than data from this study for chrons C13r–C16n.1r. This suggests that while the tuning of both the ATPS06 and the PEAT records to the 405 kyr cycle appears to be correct at least back to 35.6 Ma, there may be some inconsistencies in the tuning of shorter Milankovitch frequencies and/or the placement of chron boundaries in both the tuned records and the Umbria-Marche succession.

6. Conclusions

The $^{206}Pb/^{238}U$ dating of zircons from volcanic layers (BRLs) intercalated in the Umbria-Marche sedimentary succession indicates that published $^{40}Ar/^{39}Ar$ data from the Massignano and Monte Cagnero records are anomalously old by up to 0.4–0.5 Myr. In turn, $^{206}Pb/^{238}U$-calibrated Oligocene magnetic reversal ages from Monte Cagnero are in good agreement with the ATPS06 age model of Pälike et al. (2006), which eliminates the approximately 600 kyr Oligocene discrepancy reported between radio-isotopic and astronomically tuned age models in GTS12. We report an age of 34.09 ± 0.08 Ma for the LO of hantkeninids at Massignano, which marks the GSSP for the base of the Oligocene, and 28.11 ± 0.17 Ma for the LCO of *C. cubensis* at Monte Cagnero, a proposed site for the GSSP of the Chattian. While astronomical tuning presents undeniable advantages in terms of quantifying the distribution of time in the stratigraphic record at a 10^4 year resolution, independent dating should be used to validate short astronomical time scales (approximately <5 Myr), where the expression of longer (>405 kyr) Milankovitch frequencies, amplitude modulations, and hierarchic cycle patterns may not be adequately assessed. Crucially, this study highlights the need to integrate data from multiple dating methods to insure the accuracy of time scales underpinning Paleogene proxy records.

Acknowledgments
This work was funded through the European Community's Seventh Framework Program (FP7/2007–2013) under grant agreement 215458 and NIGFSC award IP-1228-1110. Samples MCA-123.1 and MCA-142.8 were provided by Rodolfo Coccioni. Samples from the BRL discussed in this paper are stored at the British Geological Survey, and zircon U-Pb data are archived in the Geochron database (www.geochron.org). We thank Christian Zeeden, Heiko Pälike, and an anonymous reviewer for their constructive and encouraging comments.

References

Alvarez, W., & Montanari, A. (1988). The Scaglia limestones (Late Cretaceous-Oligocene) in the northeastern Apennines carbonate sequence: Stratigraphic context and geological significance. In I. Premoli Silva, R. Coccioni, & A. Montanari (Eds.), *The Eocene-Oligocene boundary in the Marche-Umbria basin (Italy)* (pp. 13–29). International Subcommission on Paleogene Stratigraphy.

Berggren, W. A., Kent, D. V., Flynn, J. J., & Van Couvering, J. A. (1985). Cenozoic geochronology. *Bulletin Geological Society of America*, *96*(11), 1407–1418. https://doi.org/10.1130/0016-7606(1985)96%3C1407:CG%3E2.0.CO;2

Bice, D. M., & Montanari, A. (1988). Magnetic stratigraphy of the Massignano section across the Eocene-Oligocene boundary. In I. Premoli Silva, R. Coccioni, & A. Montanari (Eds.), *The Eocene-Oligocene boundary in the Marche-Umbria basin (Italy)* (pp. 111–117). International Subcommission on Paleogene Stratigraphy.

Blaauw, M., & Christen, J. A. (2005). Radiocarbon peat chronologies and environmental change. *Journal of the Royal Statistical Society: Series C (Applied Statistics)*, *54*(4), 805–816. https://doi.org/10.1111/j.1467-9876.2005.00516.x

Bowring, J. F., McLean, N. M., & Bowring, S. A. (2011). Engineering cyber infrastructure for U-Pb geochronology: Tripoli and U-Pb_Redux. *Geochemistry, Geophysics, Geosystems*, *12*, Q0AA19. https://doi.org/10.1029/2010GC003479

Bronk Ramsey, C. (2000). Comment on "The use of Bayesian statistics for ^{14}C dates of chronologically ordered samples: A critical analysis,". *Radiocarbon*, *42*(2), 199–202. https://doi.org/10.1017/S0033822200059002

Bronk Ramsey, C. (2008). Deposition models for chronological records. *Quaternary Science Reviews*, *27*, 42–60. https://doi.org/10.1016/j.quascirev.2007.01.019

Brown, R. E., Köberl, C., Montanari, A., & Bice, D. M. (2009). Evidence for a change in Milankovitch forcing caused by extraterrestrial events at Massignano, Italy, Eocene-Oligocene boundary GSSP. In C. Köberl, & A. Montanari (Eds.), *Late Eocene Earth: Hothouse Icehouse and Impacts* (Vol. 452, pp. 119–137). https://doi.org/10.1130/2009.2452(08)

Cande, S. C., & Kent, D. V. (1992). A new geomagnetic polarity time scale for the Late Cretaceous and Cenozoic. *Journal of Geophysical Research*, *97*(B10), 13917–13951. https://doi.org/10.1029/92JB01202

Cande, S. C., & Kent, D. V. (1995). Revised calibration of the geomagnetic polarity timescale for the Late Cretaceous and Cenozoic. *Journal of Geophysical Research*, *100*(B4), 6093–6095. https://doi.org/10.1029/94JB03098

Channell, J. E. T., Hodell, D. A., Singer, B. S., & Xuan, C. (2010). Reconciling astrochronological and $^{40}Ar/^{39}Ar$ ages for the Matuyama-Brunhes boundary and late Matuyama chron. *Geochemistry, Geophysics, Geosystems*, *11*, Q0AA12. https://doi.org/10.1029/2010GC003203

Charles, A. J., Condon, D. J., Harding, I. C., Pälike, H., Marshall, J. E., Cui, Y., … Croudace, I. W. (2011). Constraints on the numerical age of the Paleocene-Eocene boundary. *Geochemistry, Geophysics, Geosystems*, *12*, Q0AA17. https://doi.org/10.1029/2010GC003426

Christen, J. A., & Perez, S. (2009). A new robust statistical model for radiocarbon data. *Radiocarbon*, *51*(3), 1047–1059.

Coccioni, R., Monaco, P., Monechi, S., Nocchi, M., & Parisi, G. (1988). Biostratigraphy of the Eocene-Oligocene boundary at Massignano (Ancona, Italy). In I. Premoli Silva, R. Coccioni, & A. Montanari (Eds.), *The Eocene-Oligocene bondary in the Marche-Umbria basin (Italy)* (pp. 59–80). International Subcommission on Paleogene Stratigraphy.

Coccioni, R., & Galeotti, S. (2003). Deep-water benthic foraminiferal events from the Massignano Eocene/Oligocene boundary stratotype section and point (central Italy): Biostatigraphic, paleoecologic and paleoeanographic implications. In D. R. Prothero, L. Ivany, & E. A. Nesbitt (Eds.), *From greenhouse to icehouse: The marine Eocene-Oligocene transition* (pp. 438–452). New York: Columbia University Press.

Coccioni, R., Marsili, A., Montanari, A., Bellanca, A., Neri, R., Bice, D. M., … Williams, G. L. (2008). Integrated stratigraphy of the Oligocene pelagic sequence in the Umbria-Marche basin (northeastern Apennines, Italy): A potential Global Stratotype Section and Point (GSSP) for the Rupelian/Chattian boundary. *Bulletin Geological Society of America*, *120*(3–4), 487–511. https://doi.org/10.1130/B25988.1

Coccioni, R., Sideri, M., Bancalà, G., Catanzariti, R., Frontalini, F., Jovane, L., … Savian, J. (2012). Integrated stratigraphy (magneto-, bio- and chronostratigraphy) and geochronology of the Palaeogene pelagic succession of the Umbria-Marche Basin (central Italy). *Geological Society - Special Publications*, *373*. https://doi.org/10.1144/SP373.4

Condon, D. J., Schoene, B., McLean, N. M., Bowring, S. A., & Parrish, R. R. (2015). Metrology and traceability of U-Pb isotope dilution geochronology (EARTHTIME Tracer Calibration Part I). *Geochimica et Cosmochimica Acta*, *164*, 464–480. https://doi.org/10.1016/j.gca.2015.05.026

Davydov, V. I., Crowley, J. L., Schmitz, M. D., & Poletaev, V. I. (2010). High-precision U-Pb zircon age calibration of the global Carboniferous time scale and Milankovitch band cyclicity in the Donets Basin, eastern Ukraine. *Geochemistry, Geophysics, Geosystems*, *11*, Q0AA04. https://doi.org/10.1029/2009GC002736

Dunn, R. E., Madden, R. H., Kohn, M. J., Schmitz, M. D., Strömberg, C. A. E., Carlini, A. A., … Crowley, J. (2012). A new chronology for middle Eocene-early Miocene South American land mammal ages. *Geological Society of America Bulletin*, *125*(3–4), 539–555. https://doi.org/10.1130/B30660

Hercman, H., & Pawlak, J. (2012). MOD-AGE: An age-depth model construction algorithm. *Quaternary Geochronology*, *12*, 1–10. https://doi.org/10.1016/j.quageo.2012.05.003

Hess, J., Stott, L. D., Bender, M. L., Kennett, J. P., & Schilling, J.-G. (1989). The Oligocene marine microfossil record: Age assessments using strontium isotopes. *Paleoceanography*, *4*(6), 655–679. https://doi.org/10.1029/PA004i006p00655

Hilgen, F. J., & Kuiper, K. F. (2009). A critical evaluation of the numerical age of the Eocene-Oligocene boundary. In C. Köberl, & A. Montanari (Eds.), *Late Eocene Earth: Hothouse icehouse and impacts* (pp. 139–148). https://doi.org/10.1130/2009.2452(09)

Hilgen, F. J., Kuiper, K. F., & Lourens, L. J. (2010). Evaluation of the astronomical time scale for the Paleocene and earliest Eocene. *Earth and Planetary Science Letters*, *300*(1–2), 139–151. https://doi.org/10.1016/j.epsl.2010.09.044

Hora, J. M., Singer, B. S., Jicha, B. R., Beard, B. L., Johnson, C. M., de Silva, S., & Salisbury, M. (2010). Volcanic biotite-sanidine $^{40}Ar/^{39}Ar$ age discordances reflect Ar partitioning and pre-eruption closure in biotite. *Geology*, *38*(10), 923–926. https://doi.org/10.1130/G31064.1

Hyland, E., Murphy, B., Varela, P., Marks, K., Colwell, L., Tori, … Montanari, A. (2009). Integrated stratigraphic and astrochronologic calibration of the Eocene-Oligocene transition in the Monte Cagnero section (northeastern Apennines, Italy): A potential parastratotype for the Massignano Global Stratotype Section and Point (GSSP). In C. Köberl, & A. Montanari (Eds.), *Late Eocene Earth: Hothouse icehouse and impacts* (pp. 303–322). https://doi.org/10.1130/2009.2452(19)

Jaffey, A. H., Flynn, K. F., Glendeni.Le, Bentley, W. C., & Essling, A. M. (1971). Precision measurement of half-lives and specific activities of U-235 and U-238. *Physics Review*, *4*(5), 1889. https://doi.org/10.1103/PhysRevC.4.1889

Jovane, L., Florindo, F., & Dinares-Turell, J. (2004). Environmental magnetic record of paleoclimate change from the Eocene-Oligocene stratotype section, Massignano, Italy. *Geophysical Research Letters*, *31*, L15601. https://doi.or/10.1029/2004GL020554

Jovane, L., Florindo, F., Sprovieri, M., & Pälike, H. (2006). Astronomic calibration of the late Eocene/early Oligocene Massignano section (central Italy). *Geochemistry, Geophysics, Geosystems*, *7*, Q07012. https://doi.org/10.1029/2005GC001195

Jovane, L., Savian, J. F., Coccioni, R., Frontalini, F., Bancalà, G., Catanzariti, R., … Florindo, F. (2013). Integrated magnetobiostratigraphy of the middle Eocene-lower Oligocene interval from the Monte Cagnero section, central Italy. *Geological Society - Special Publications*, *373*. https://doi.org/10.1144/SP373.13

Jovane, L., Sprovieri, M., Coccioni, R., Florindo, F., Marsili, A., & Laskar, J. (2010). Astronomical calibration of the middle Eocene Contessa Highway section (Gubbio, Italy). *Earth and Planetary Science Letters*, *298*(1–2), 77–88. https://doi.org/10.1016/j.epsl.2010.07.027

Jovane, L., Sprovieri, M., Florindo, F., Acton, G., Coccioni, R., Dall'Antonia, B., & Dinarès-Turell, J. (2007). Eocene-Oligocene paleoceanographic changes in the stratotype section, Massignano, Italy: Clues from rock magnetism and stable isotopes. *Journal of Geophysical Research*, *112*, B11101. https://doi.org/10.1029/2007JB004963

Kuiper, K. F., Deino, A., Hilgen, F. J., Krijgsman, W., Renne, P. R., & Wijbrans, J. R. (2008). Synchronizing rock clocks of Earth history. *Science*, *320*(5875), 500–504. https://doi.org/10.1126/science.1154339

Lanci, L., Lowrie, W., & Montanari, A. (1996). Magnetostratigraphy of the Eocene/Oligocene boundary in a short drill-core. *Earth and Planetary Science Letters*, *143*(1–4), 37–48. https://doi.org/10.1016/0012-821X(96)00136-7

Laskar, J., Fienga, A., Gastineau, M., & Manche, H. (2011). La2010: A new orbital solution for the long-term motion of the Earth. *Astronomy and Astrophysics*, *532*, A89. https://doi.org/10.1051/0004-6361/201116836

Laskar, J., Robutel, P., Joutel, F., Gastineau, M., Correia, A. C. M., & Levrard, B. (2004). A long-term numerical solution for the insolation quantities of the Earth. *Astronomy and Astrophysics*, *428*(1), 261–285. https://doi.org/10.1051/0004-6361:20041335

Leckie, R. M., Farnham, C., & Schmidt, M. G. (1993). Oligocene planktonic foraminifer biostratigraphy of Hole 803D (Ontong Java Plateau) and Hole 628A (Little Bahama Bank) and comparison with the southern high latitudes. *Proceedings Ocean Drilling Program Scientific Results*, *130*. https://doi.org/10.2973/odp.proc.sr.130.012.1993

Liebrand, D., Beddow, H. M., Lourens, L. J., Pälike, H., Raffi, I., Bohaty, S. M., … Batenburg, S. J. (2016). Cyclostratigraphy and eccentricity tuning of the early Oligocene through early Miocene (30.1–17.1 Ma): *Cibicides mundulus* stable oxygen and carbon isotope records from Walvis Ridge Site 1264. *Earth and Planetary Science Letters*, *450*, 392–405. https://doi.org/10.1016/j.epsl.2016.06.007

Lourens, L., Hilgen, F., Shackleton, N. J., Laskar, J., & Wilson, D. (2004). The Neogene period. In F. M. Gradstein, J. G. Ogg, & A. Smith (Eds.), *A geologic time scale 2004* (pp. 409–440). Cambridge University Press. https://doi.org/10.1017/CBO9780511536045

Lowrie, W., & Lanci, L. (1994). Magnetostratigraphy of the Eocene-Oligocene boundary sections in Italy—No evidence for short subchrons within 12r and 13r. *Earth and Planetary Science Letters*, *126*(4), 247–258. https://doi.org/10.1016/0012-821X(94)90110-4

Machlus, M., Hemming, S. R., Olsen, P. E., & Christie-Blick, N. (2004). Eocene calibration of geomagnetic polarity time scale reevaluated: Evidence from the Green River formation of Wyoming. *Geology*, *32*(2), 137–140. https://doi.org/10.1130/G20091.1

Mattinson, J. M. (2005). Zircon U-Pb chemical abrasion ("CA–TIMS") method: Combined annealing and multi-step partial dissolution analysis for improved precision and accuracy of zircon ages. *Chemical Geology*, *220*(1–2), 47–66. https://doi.org/10.1016/j.chemgeo.2005.03.011

McLean, N. M., Bowring, J. F., & Bowring, S. A. (2011). An algorithm for U-Pb isotope dilution data reduction and uncertainty propagation. *Geochemistry, Geophysics, Geosystems*, *12*, Q0AA18. https://doi.org/10.1029/2010GC003478

McLean, N. M., Condon, D. J., Schoene, B., & Bowring, S. A. (2015). Evaluating uncertainties in the calibration of isotopic reference materials and multi-element isotopic tracers (EARTHTIME Tracer Calibration Part II). *Geochimica et Cosmochimica Acta*, *164*, 481–501. https://doi.org/10.1016/j.gca.2015.02.040

Meyers, S. R., Siewert, S. E., Singer, B. S., Sageman, B. B., Condon, D. J., Obradovich, J. D., … Sawyer, D. A. (2012). Intercalibration of radioisotopic and astrochronologic time scales for the Cenomanian-Turonian boundary interval, Western Interior Basin, USA. *Geology*, *40*(1), 7–10. https://doi.org/10.1130/G32261.1

Miller, K. G., Aubry, M. P., Khan, M. J., Melillo, A. J., Kent, D. V., & Berggren, W. A. (1985). Oligocene-Miocene biostratigraphy, magnetostratigraphy, and isotopic stratigraphy of the western North Atlantic. *Geology*, *13*(4), 257–261. https://doi.org/10.1130/0091-7613(1985)13%3c257:OBMAIS%3e2.0.CO;2

Min, K. W., Mundil, R., Renne, P. R., & Ludwig, K. R. (2000). A test for systematic errors in $^{40}Ar/^{39}Ar$ geochronology through comparison with U/Pb analysis of a 1.1 Ga rhyolite. *Geochimica et Cosmochimica Acta*, *64*(1), 73–98. https://doi.org/10.1016/S0016-7037(99)00204-5

Montanari, A., Deino, A. L., Drake, R. E., Turrin, B. D., DePaolo, D. J., Odin, G. S., … Bice, D. M. (1988). Radioisotopic dating of the Eocene-Oligocene boundary in the pelagic sequence of the northeastern Appenines. In I. Premoli Silva, R. Coccioni, & A. Montanari (Eds.), *The Eocene-Oligocene boundary in the Marche-Umbria basin (Italy)* (pp. 195–208). International Subcommission on Paleogene Stratigraphy.

Montanari, A., Drake, R., Bice, D. M., Alvarez, W., Curtis, G. H., Turrin, B. D., & DePaolo, D. J. (1985). Radiometric time scale for the upper Eocene and Oligocene based on K/Ar and Rb/Sr dating of volcanic biotites from the pelagic sequence of Gubbio, Italy. *Geology*, *13*(9), 596–599. https://doi.org/10.1130/0091-7613(1985)13%3C596:RTSFTU%3E2.0.CO;2

Mundil, R., Ludwig, K. R., Metcalfe, I., & Renne, P. R. (2004). Age and timing of the Permian mass extinctions: U/Pb dating of closed-system zircons. *Science*, *305*(5691), 1760–1763. https://doi.org/10.1126/science.1101012

Oberli, F., & Meier, M. (1991). Age of the Eocene-Oligocene boundary in the Marche-Umbria basin, Italy, by high resolution U-Th-Pb dating. *Terrain*, *3*(1), 286.

Odin, G. S., Barbin, V., Hurford, A. J., Baadsgaard, H., Galbrun, B., & Gillot, P. Y. (1991). Multimethod radiometric dating of volcano-sedimentary layers from northern Italy—Age and duration of the Priabonian stage. *Earth and Planetary Science Letters*, *106*(1–4), 151–168. https://doi.org/10.1016/0012-821X(91)90069-T

Odin, G. S., Montanari, A., Deino, A., Drake, R., Guise, P. G., Kreuzer, H., & Rex, D. C. (1991). Reliability of volcano-sedimentary biotite ages across the Eocene-Oligocene boundary. *Chemical Geology*, *86*(3), 203–224. https://doi.org/10.1016/0168-9622(91)90050-7

Ogg, J. G., & Smith, A. G. (2004). The geomagnetic polarity time scale. In F. M. Gradstein, J. G. Ogg, & A. G. Smith (Eds.), *A geologic time scale 2004* (pp. 63–86). Cambridge University Press. https://doi.org/10.1017/CBO9780511536045

Paine, J. H., Nomade, S., & Renne, P. R. (2006). Quantification of ^{39}Ar recoil ejection from GA1550 biotite during neutron irradiation as a function of grain dimensions. *Geochimica et Cosmochimica Acta*, *70*(6), 1507–1517. https://doi.org/10.1016/j.gca.2005.11.012

Pälike, H., Norris, R. D., Herrle, J. O., Wilson, P. A., Coxall, H. K., Lear, C. H., … Wade, B. S. (2006). The heartbeat of the Oligocene climate system. *Science*, *314*(5807), 1894–1898. https://doi.org/10.1126/science.1133822

Pälike, H., Shackleton, N. J., & Röhl, U. (2001). Astronomical forcing in late Eocene marine sediments. *Earth and Planetary Science Letters*, *193*(3–4), 589–602. https://doi.org/10.1016/S0012-821X(01)00501-5

Poore, R. Z., Tauxe, L., Percival, S. F. L. Jr., Labrecque, J., Wright, R., Petersen, N. P., … Hsu, K. J. (1983). Late Cretaceous-Cenozoic magnetostratigraphic and biostratigraphic correlations of the South Atlantic Ocean: DSDP Leg 73. *Palaeogeography Palaeoclimatology Palaeoecology*, *42*, 127–149. https://doi.org/10.1016/0031-0182(83)90041-X

Premoli Silva, I., & Jenkins, D. G. (1993). Decision on the Eocene-Oligocene boundary stratotype. *Episodes*, *16*(3), 379–382.

Pujol, C. (1983). Cenozoic planktonic foraminiferal biostratigraphy of the southwestern Atlantic (Rio Grande Rise) Deep Sea Drilling Project Leg 72: Initial rep. *Deep Sea*, *72*, 623–673. https://doi.org/10.2973/dsdp.proc.72.129.1983

Renne, P. R., Deino, A. L., Hilgen, F. J., Kuiper, K. F., Mark, D. F., Mitchell, W. S., … Smit, J. (2013). Time scales of critical events around the Cretaceous-Paleogene boundary. *Science*, *339*, 684–687. https://doi.org/10.1126/science.1230492

Renne, P. R., Deino, A. L., Walter, R. C., Turrin, B. D., Swisher, C. C., Becker, T. A., … Jaouni, A. R. (1994). Intercalibration of astronomical and radioisotopic time. *Geology*, *22*(9), 783–786. https://doi.org/10.1130/0091-7613(1994)022%3C0783:IOAART%3E2.3.CO;2

Renne, P. R., Mundil, R., Balco, G., Min, K., & Ludwig, K. R. (2010). Joint determination of ^{40}K decay constants and $^{40}Ar^*/^{40}K$ for the Fish Canyon sanidine standard, and improved accuracy for $^{40}Ar/^{39}Ar$ geochronology. *Geochimica et Cosmochimica Acta*, *74*, 5349–5367. https://doi.org/10.1016/j.gca.2010.06.017

Renne, P. R., Swisher, C. C., Deino, A. L., Karner, D. B., Owens, T. L., & DePaolo, D. J. (1998). Intercalibration of standards, absolute ages and uncertainties in $^{40}Ar/^{39}Ar$ dating. *Chemical Geology*, *145*, 117–152. https://doi.org/10.1016/S0009-2541(97)00159-9

Rivera, T. A., Storey, M., Zeeden, C., Hilgen, F. J., & Kuiper, K. F. (2011). A refined astronomically calibrated $^{40}Ar/^{39}Ar$ age for Fish Canyon sanidine. *Earth and Planetary Science Letters*, *311*, 420–426. https://doi.org/10.1016/j.epsl.2011.09.017

Sageman, B. B., Singer, B. S., Meyers, S. R., Siewert, S. E., Walaszczyk, I., Condon, D. J., … Sawyer, D. A. (2014). Integrating $^{40}Ar/^{39}Ar$, U-Pb, and astronomical clocks in the Cretaceous Niobrara formation, Western Interior Basin, USA. *Bulletin Geological Society of America*, *126*(7–8), 956–973. https://doi.org/10.1130/B30929.1

Sahy, D., Condon, D. J., Terry, D. O., Fischer, A. U., & Kuiper, K. F. (2015). Synchronizing terrestrial and marine records of environmental change across the Eocene-Oligocene transition. *Earth and Planetary Science Letters*, *427*, 171–182. https://doi.org/10.1016/j.epsl.2015.06.057

Schmitz, M. D. (2012). Chapter 6 - Radiogenic isotope geochronology. In F. M. Gradstein, et al. (Eds.), *The Geological Time Scale 2012* (pp. 115–126). Elsevier. https://doi.org/10.1016/B978-0-444-59425-9.00006-8

Schoene, B., Condon, D. J., Morgan, L., & McLean, N. (2013). Precision and accuracy in geochronology. *Elements*, *9*(1), 19–24. https://doi.org/10.2113/gselements.9.1.19

Schoene, B., Guex, J., Bartolini, A., Schaltegger, U., & Blackburn, T. J. (2010). Correlating the end-Triassic mass extinction and flood basalt volcanism at the 100 ka level. *Geology*, *38*(5), 387–390. https://doi.org/10.1130/G30683.1

Scholz, D., & Hoffmann, D. L. (2011). StalAge—An algorithm designed for construction of speleothem age models. *Quaternary Geochronology*, *6*(3–4), 369–382. https://doi.org/10.1016/j.quageo.2011.02.002

Shackleton, N. J., Hall, M. A., Raffi, I., Tauxe, L., & Zachos, J. (2000). Astronomical calibration age for the Oligocene-Miocene boundary. *Geology*, *28*(5), 447–450. https://doi.org/10.1130/0091-7613(2000)28%3C447:ACAFTO%3E2.0.CO;2

Shackleton, N. J., & Kennett, P. (1975). Paleotemperature history of the Cenozoic and the initiation of Antarctic glaciation: Oxygen and carbon analyses in DSDP Sites 277, 279, and 281, Initial Rep. *Deep Sea*, *29*, 743–755. https://doi.org/10.2973/dsdp.proc.29.117.1975

Singer, B. S. (2014). A Quaternary geomagnetic instability time scale. *Quaternary Geochronology*, *21*, 29–52. https://doi.org/10.1016/j.quageo.2013.10.003

Smith, M. E., Chamberlain, K. R., Singer, B. S., & Carroll, A. R. (2010). Eocene clocks agree: Coeval $^{40}Ar/^{39}Ar$, U-Pb, and astronomical ages from the Green River formation. *Geology*, *38*(6), 527–530. https://doi.org/10.1130/G30630.1

Spell, T. L., & McDougall, I. (2003). Characterization and calibration of $^{40}Ar/^{39}Ar$ dating standards. *Chemical Geology*, *198*(3–4), 189–211. https://doi.org/10.1016/S0009-2541(03)00005-6

Swisher, C. C., Dingus, L., & Butler, R. F. (1993). $^{40}Ar/^{39}Ar$ dating and magnetostratigraphic correlation of the terrestrial Cretaceous-Paleogene boundary and Puercan mammal age, Hell Creek-Tullock formations, eastern Montana. *Canadian Journal of Earth Sciences*, *30*(9), 1981–1996. https://doi.org/10.1139/e93-174

Swisher, C. C., & Prothero, D. R. (1990). Single-crystal $^{40}Ar/^{39}Ar$ dating of the Eocene-Oligocene transition in North America. *Science*, *249*, 760–762. https://doi.org/10.1126/science.249.4970.760

Van Simaeys, S., Man, E. D., Vandenberghe, N. l., Brinkhuis, H., & Steurbaut, E. (2004). Stratigraphic and palaeoenvironmental analysis of the Rupelian-Chattian transition in the type region: Evidence from dinoflagellate cysts, foraminifera and calcareous nannofossils. *Palaeogeography Palaeoclimatology Palaeoecology*, *208*(1–2), 31–58. https://doi.org/10.1016/j.palaeo.2004.02.029

Vandenberghe, N., Hilgen, F. J., Speijer, R. P., Ogg, J. G., Gradstein, F. M., Hammer, O., … Hooker, J. J. (2012). The Paleogene period. In F. M. Gradstein, J. G. Ogg, M. D. Schmitz, & G. M. Ogg (Eds.), *The geologic time scale 2012* (pp. 855–921). Boston: Elsevier. https://doi.org/10.1016/B978-0-444-59425-9.00028-7

Wade, B. S., Berggren, W. A., & Olsson, R. K. (2007). The biostratigraphy and paleobiology of Oligocene planktonic foraminifera from the equatorial Pacific Ocean (ODP Site 1218). *Marine Micropaleontology*, *62*(3), 167–179. https://doi.org/10.1016/j.marmicro.2006.08.005

Wade, B. S., Pearson, P. N., Berggren, W. A., & Pälike, H. (2011). Review and revision of Cenozoic tropical planktonic foraminiferal biostratigraphy and calibration to the geomagnetic polarity and astronomical time scale. *Earth-Science Reviews*, *104*(1–3), 111–142. https://doi.org/10.1016/j.earscirev.2010.09.003

Wendt, I., & Carl, C. (1991). The statistical distribution of the mean squared weighted deviation. *Chemical Geology*, *86*(4), 275–285. https://doi.org/10.1016/0168-9622(91)90010-T

Westerhold, T., & Röhl, U. (2009). High resolution cyclostratigraphy of the early Eocene—New insights into the origin of the Cenozoic cooling trend, Clim. *Pastoralism*, *5*(3), 309–327. https://doi.org/10.5194/cp-5-309-2009

Westerhold, T., Röhl, U., Frederichs, T., Bohaty, S. M., & Zachos, J. C. (2015). Astronomical calibration of the geological timescale: Closing the middle Eocene gap. *Climate of the Past*, *11*, 1181–1195. https://doi.org/10.5194/cp-11-1181-2015

Westerhold, T., Röhl, U., Laskar, J., Raffi, I., Bowles, J., Lourens, L. J., & Zachos, J. C. (2007). On the duration of magnetochrons C24r and C25n and the timing of early Eocene global warming events: Implications from the Ocean Drilling Program Leg 208 Walvis Ridge depth transect. *Paleoceanography*, *22*, PA2201. https://doi.org/10.1029/2006PA001322

Westerhold, T., Röhl, U., Pälike, H., Wilkens, R., Wilson, P. A., & Acton, G. (2013). Orbitally tuned time scale and astronomical forcing in the middle Eocene to early Oligocene. *Climate of the Past*, *10*, 955–973. https://doi.org/10.5194/cp-10-955-2014

Westerhold, T., Röhl, U., Raffi, I., Fornaciari, E., Monechi, S., Reale, V., … Evans, H. F. (2008). Astronomical calibration of the Paleocene time. *Palaeogeography Palaeoclimatology Palaeoecology*, *257*(4), 377–403. https://doi.org/10.1016/j.palaeo.2007.09.016

Wotzlaw, J.-F., Schaltegger, U., Frick, D. A., Dungan, M. A., Gerdes, A., & Günther, D. (2013). Tracking the evolution of large-volume silicic magma reservoirs from assembly to supereruption. *Geology*, *41*(8), 867–870. https://doi.org/10.1130/G34366.1

Zachos, J., Pagani, M., Sloan, L., Thomas, E., & Billups, K. (2001). Trends, rhythms, and aberrations in global climate 65 Ma to present. *Science*, *292*(5517), 686–693. https://doi.org/10.1126/science.1059412

Zanazzi, A., Kohn, M. J., MacFadden, B. J., & Terry, D. O. (2007). Large temperature drop across the Eocene-Oligocene transition in central North America. *Nature*, *445*(7128), 639–642. https://doi.org/10.1038/nature05551